Spatial and Temporal Variations of Gravity Wave Parameters. Part I: Intrinsic Frequency, Wavelength, and Vertical Propagation Direction

Ling Wang [1], and Marvin A. Geller

Institute for Terrestrial and Planetary Atmospheres, State University of New York at Stony Brook, Stony Brook, NY 11794-5000

M. Joan Alexander

Colorado Research Associates Division, NorthWest Research Associates, Inc., Boulder, Colorado, 80301

(Submitted to *J. Atmos. Sci.*)

[1]Current affiliation: Colorado Research Associates Division, NorthWest Research Associates, Inc., Boulder, Colorado 80301

Corresponding author address: Ling Wang, Colorado Research Associates Division, NorthWest Research Associates, Inc., 3380, Mitchell Lane Boulder, CO 80301, e-mail: lwang@cora.nwra.com

Abstract

Five years (1998-2002) of U.S. high vertical resolution radiosonde data have been analyzed to derive important gravity wave parameters such as intrinsic frequency, vertical and horizontal wavelengths, and the vertical propagation direction.

Intrinsic frequencies increase with increasing latitude in both the troposphere and lower stratosphere, with larger values in the troposphere. In the lower stratosphere, the intrinsic frequency is higher in winter and lower in summer, especially at mid- and high-latitudes. Intrinsic frequencies divided by the Coriolis parameter f are around 4 in the troposphere, and 2.4-3 in the lower stratosphere. In the lower stratosphere, $\hat{\omega}/f$ generally decreases weakly with increasing latitude.

Most dominant vertical wavelengths decrease with increasing latitude in the lower stratosphere, and they maximize at mid-latitudes (35°-40°N) in the troposphere. In both the troposphere and lower stratosphere, vertical wavelengths are generally longer in winter and shorter in summer.

Most dominant horizontal wavelengths decrease with increasing latitude in both the troposphere and lower stratosphere, with larger values in the lower stratosphere.

Approximately 50% of the tropospheric gravity waves show upward energy propagation, whereas there is about 75% upward energy propagation in the lower stratosphere, indicating that some waves might be generated in the upper troposphere and/or that tropospheric reflections of gravity waves are occurring. The lower stratospheric fraction of upward energy propagation is generally smaller in winter and bigger in summer, especially at mid- and high-latitudes.

Interpretations are given for some of the results whereas other results remain to be explained.

1. Introduction

Atmospheric gravity waves play significant roles in the reversal of the temperature gradient at the mesopause and the formation of the winter warm mesopause (Houghton 1978). They are also important in affecting the stratospheric temperature distribution and play a role in determining the residual mean meridional circulation via downward control (Haynes et al. 1991; Holton et al. 1995). The effects of gravity waves have to be parameterized or resolved explicitly (which is computationally demanding) in GCM's to obtain realistic mean atmospheric circulations and temperature distributions.

Currently, most GCMs that extend through the middle atmosphere parameterize nonorographic gravity waves by specifying a constant gravity wave source spectrum at a certain altitude. Observational studies, however, have found that gravity wave activity varies significantly both temporally and spatially (Hirota 1984; Fetzer and Gille 1994; Eckermann et al. 1995; Allen and Vincent 1995; Eckermann and Preusse 1999; Tsuda et al. 2000; McLandress et al. 2000; Wang and Geller 2003). Wang and Geller (2003) derived short vertical wavelength gravity wave morphology from four years (1998-2001) of U.S. high vertical resolution radiosonde data. They found the gravity wave variance in these data is stronger in DJF and weaker in JJA at all latitudes in both the lower stratosphere and troposphere, and it decreases poleward in the lower stratosphere whereas it maximizes at mid-latitudes (35°-40°N) in the troposphere.

Only recently have a few studies utilized spatially varying gravity wave source spectra in GCM's. For example, Manzini and McFarlane (1998) compared two simulations from the ECHAM4 model in which the gravity wave spectra were launched at

two different heights and had a latitudinal dependence in the characteristic horizontal wavenumber, and they found noteworthy differences in the simulated middle atmospheres. Medvedev, Klaassen and Beagley (1998) showed that an anisotropic gravity wave source significantly improves the middle atmosphere circulation compared to an isotropic one. Scaife et al. (2000) specified a gravity wave source spectrum with latitudinally varying momentum flux in the tropics and obtained a more realistic simulation of the stratospheric quasi-biennial oscillation.

As will be shown in the subsequent sections of this paper, the intrinsic frequencies, vertical and horizontal wavelengths, and vertical propagation directions derived from the U.S. high resolution radiosonde data, all exhibit distinctive spatial and temporal patterns. In a companion paper, we will show that horizontal propagation directions also show certain spatial and temporal variations, and we will examine the QBO effects on the temporal variations of gravity wave energies and momentum fluxes at low latitudes. These characteristic patterns can be due to the gravity wave dispersion relation, wave intermittency and energy propagation effects, and/or source characteristics. In this paper, we try to see which of these effects account for the various observations. We believe that such studies can help to specify more realistic gravity wave source spectra for use in GCMs.

The paper is organized as follows: section 2 describes briefly the data and analysis method; section 3 shows the spatial and temporal distributions of gravity wave parameters including intrinsic frequency divided by the Coriolis parameter f, vertical wavelength, horizontal wavelength, and vertical energy propagation direction; discussion is given in section 4; in the final section, the summary and conclusions are given.

2. Data and Methods

Data

The data used in this study are the U.S. rawinsonde 6-second resolution data from the National Oceanic and Atmospheric Administration (NOAA) National Climatic Data Center (NCDC) for the years of 1998, 1999, 2000, 2001, and 2002. Both temperature and horizontal wind soundings are available in the data set. For the temperature measurement, V*äsälä* RS-80 series ($\sim 70\%$ of the stations) and VIZ B2 series ($\sim 30\%$ of the stations) radiosondes were used. The accuracy is about $0.2°K$ for the former, and $\sim 0.3°K$ for the latter. For all but one of the stations, the winds were estimated from the elevations and azimuthal angles of the radiosondes which were measured by tracking the position of the balloons using the 6-second Micro-ART system (Williams et al. 1993). The accuracy for the winds derived from this system is not a constant but it is generally around 1 ms^{-1} for most of the soundings. For Charleston, SC (32.9°N, 280.0°E), the Loran-C windfinding system (NEXUS) was used to determine the wind speeds and the accuracy of this system is believed to be a fraction of a meter per second.

The location map of the radiosonde stations has been given in Wang and Geller (2003) in which the morphology of gravity wave energies from four years (1998-2001) of the data is presented. As a reference, Table 1 lists the names and locations of all the high vertical resolution radiosonde stations. There are 94 stations in total, located across the contiguous United States, Alaska, Hawaii, Caribbean islands, and western tropical Pacific islands. The stations cover a very wide area with a latitude range from 14°S to 71°N and a longitude range from 135°E to 305°E, and cover diverse terrain

ranging from tropical islands, to mid-continent plains, to mountains, to the Arctic. Therefore, the data can be used to investigate gravity waves from diverse sources and under different propagation conditions. With five year's data being available, the data can also be used to examine gravity wave interannual variations.

Note that four of the stations (Corpus Christi, TX, 27.8°N, 262.5°E; Charleston, SC, 280.0°E; Salt Lake City, UT, 40.8°N, 248.0°E; Guam, Mariana Island, 13.6°N, 144.8°E) miss one or more years of data completely. Besides, there is one Southern Hemisphere station, Pago Pago International Airport (14.33°S, 14.33°E), which is located too far away from all the other stations to have it included in the latitudinal mean. As a result, only the analysis results for the remaining 89 stations will be presented in this paper.

Generally, for each of the stations, both temperature and horizontal wind data are available twice daily at 0000 and 1200 UTC (Coordinated Universal Time), although a very limited number of soundings were taken at other UTCs. Approximately half of the soundings are taken at 0000 and 1200 UTC, respectively, whereas soundings taken at other UTCs together account for less than 1% of the total soundings.

The measurements of temperature are recorded at 6-sec intervals which correspond to $\sim 30\ m$ height resolution, given that the vertical velocity of the balloon is typically about 5 ms^{-1}. Smoothing procedures are applied to derive the wind data from the raw 6-sec resolution elevation and azimuth angle data and the resulting wind data have a resolution of $\sim$150 m. See the *Data Documentation for Data Set Rawinsonde 6-second Data TD6211* (NCDC 2002) for more details about the data.

Methods

The analysis methods follow closely Allen and Vincent (1995) and Vincent et al. (1997). Basically, for each individual sounding profile, a tropospheric and a lower stratospheric segment are defined for gravity wave analysis. The tropospheric segment is chosen to be 2 to 8.9 km, except for Arctic stations (thirteen in total) where an altitude range of 2-7.4 km is chosen so as to take proper account of the much lower tropopause in the Arctic. The lower stratospheric segment is specified to be 18 to 24.9 km. Such altitude ranges are very close to what were used in Allen and Vincent (1995), i.e. 2 to 9 km in the troposphere and 17 to 24 km in the lower stratosphere. The background dry Brunt-V*äisälä* frequencies [2] are roughly constant with height over each chosen segment, which makes the interpretation of the results more straightforward (Allen and Vincent 1995).

Prior to analysis, each raw sounding profile was inspected visually. Those profiles which did not cover the whole altitude range of interest and/or had too many missing records were discarded. Profiles that had suspiciously large gradients in the wind and/or temperature profiles were also discarded. Generally, most of the stations have more than 200 valid profiles each year. The station Flagstaff, AZ (35.2°N, 248.2°E) is a notable exception. There, all of the soundings for the tropospheric segment were discarded due to the facts that the elevation of the station (2,179 m) is higher than the lowest altitude of the tropospheric segment (i.e., 2 km), and that most of the soundings have too large vertical gradient and/or large gaps, especially below 3 km (not shown).

[2] As opposed to the moist Brunt-V*äisälä* frequency (Durran and Klemp, 1982). Henceforth, they will be referred simply as Brunt-V*äisälä* frequencies for brevity.

Within each segment, the mean profiles of the zonal and meridional wind and temperature $(\overline{u}, \overline{v}, \overline{T})$ are estimated using second-order polynomial fits. The gravity wave perturbations (u', v', T') are simply the differences between the original sounding profiles and the mean profiles, i.e.

$$(u', v', T') = (u, v, T) - (\overline{u}, \overline{v}, \overline{T}) \tag{1}$$

Note that second-order polynomial fits were also used by Allen and Vincent (1995) and Vincent and Alexander (2000) to represent the mean profiles in analyzing gravity wave activity from radiosonde soundings over stations within Australia and Antarctica and over Cocos Islands (12°S, 97°E), respectively. Vincent et al. (1997) used third-order polynomial fits to estimate the mean profiles from their radiosonde wind and temperature profiles over Macquarie Island (55°S, 159°E). Tsuda et al. (2000) extracted gravity wave perturbations from each GPS/MET temperature profile by applying a high-pass filter with a cutoff at 10 km. Eckermann et al. (1994) used the same method as Tsuda et al. (2000) in their analysis of rocketsonde profiles. In analyzing radiosonde soundings over one station in Illinois, Nastrom et al. (1997) and Nastrom and VanZandt (2001) found that a linear fit was an adequate approximation of the mean profile for their purposes.

In this study, we tested linear, third-order polynomial, and fourth-order polynomial fits to estimate the background mean profiles, and the analysis results were compared with the results presented in the next section using the second-order polynomial fit. Separate analyses have also been carried out for soundings taken at 0000 and 1200 UTC, respectively. It was found that the temporal and spatial variations of gravity wave parameters (as will be presented in section 3) remained almost the same for all the different methods tested. In addition, subdivisions of the segments,

i.e., 2000-5450 m, 5450-8000 m, 18,000-21,450 m, 21,450-24,900 m, were also used for alternative analysis to those shown in the next section, and it was found that the major results to be presented in section 3 also remained essentially the same, except for the size of the dominant vertical wavelength (not shown).

For each segment, the averaged gravity wave kinetic energy per unit mass (energy density) Ke is approximated by

$$Ke = \frac{1}{2}\left(\overline{u'^2} + \overline{v'^2}\right) \tag{2}$$

and the potential energy density Pe can be approximated by

$$Pe = \frac{g^2}{2N^2}\overline{\hat{T}'^2} \tag{3}$$

where N is the Brunt-V*äisälä* frequency which is calculated directly from the data; g is the gravitational constant; $\hat{T}' = T'/\overline{T}$ is the normalized temperature fluctuation. Note that the vertical velocity contribution to Ke has been neglected in (2). In the above two equations, the overbar denotes averaging over the segment's altitude range. The segment averaged total gravity wave energy density E_t is simply the sum of Ke and Pe,

$$E_t = Ke + Pe \tag{4}$$

The intrinsic frequency $\hat{\omega}$, which is the frequency observed in a frame moving in the direction of the background wind, may be obtained from the axial-ratio of the wind hodograph which is just $|\hat{\omega}/f|$ for a monochromatic wave (Gossard and Hooke 1975). Hines (1989) suggested that a shear in the wind component transverse to the direction of propagation will change the axial-ratio, AXR. Therefore, a more accurate formula to estimate $\hat{\omega}$ can be written as

$$AXR = \left|\frac{\hat{\omega}}{f} - \frac{1}{N}\frac{dV_T}{dz}\right| \tag{5}$$

where V_T is the mean wind velocity component transverse to the direction of propagation (Vincent et al. 1997). In practice, the Stokes parameters technique (e.g., Eckermann and Vincent 1989) is used to calculate the axial-ratio, AXR.

The most dominant vertical wavenumber $\overline{m}$, which is inversely proportional to the vertical wavelength $\overline{\lambda}_z$, is estimated as the "energy-weighted" average vertical wavenumber from the normalized temperature perturbation spectrum. The most dominant horizontal wavenumber $\overline{K}$, which is inversely proportional to the horizontal wavelength $\overline{\lambda}_h$, is determined for each sounding using the gravity wave dispersion relation

$$\overline{K}^2 = \frac{(\overline{m}^2 + \alpha^2)\,(\hat{\omega}^2 - f^2)}{(N^2 - \hat{\omega}^2)} \tag{6}$$

and using the inferred values of $\hat{\omega}$ and $\overline{m}$. In (6), $\alpha = 1/2H_\rho$ and H_ρ is the density scale height.

The vertical propagation direction of gravity wave energies can be estimated from the wind data alone. According to linear gravity wave theory, the Coriolis effect causes the perturbation wind vector associated with an upward (downward) propagating gravity wave to rotate anticyclonically (cyclonically) with increasing height (e.g., Holton 1992). In other words, in the northern hemisphere, a clockwise rotation of the wind perturbation hodograph corresponds to a wave that is propagating upward, whereas an anticlockwise rotation indicates that the wave is propagating downward. The rotary-spectral technique (Vincent 1984) can be used to decompose the wind perturbation field into anticlockwise (AW) and clockwise (CW) components. The fraction of upward propagating waves is then simply the ratio of the CW (AW) to ($CW + AW$) in the northern (southern) hemisphere.

In fact, the above approach tends to underestimate the percentage of upward

propagation. It is assumed by the rotary analysis technique that the upward and downward propagating motions are circularly polarized. This assumption leads to decomposing a single upward propagating wave into an upward-propagating fraction of $(1 + f/\hat{\omega})/2$, and a downward-propagating fraction of $(1 - f/\hat{\omega})/2$ (Vincent 1984; Eckermann and Vincent 1989; Eckermann et al. 1994). When $\hat{\omega}$ is much larger than f, the approach can lead to a significant underestimate of the fraction of upward propagation. As will be shown later in this paper, the waves retrieved from the radiosonde flights are mostly low frequency waves with intrinsic frequency about 2-4 f. Thus, the discrepancy is not so serious, and meaningful results can still be obtained by this method.

Due to the limitations of the wind speed accuracy of the U.S. radiosonde data, the wind perturbation axial ratios and hence intrinsic frequencies greater than a certain value are not reliable (Vincent and Alexander 2000) and should not be included in the computations of the mean frequency and other wave parameters, such as wavelength. The threshold value of the intrinsic frequency that can be reliably determined in the analysis depends on the accuracy of the wind speeds and rms wave perturbations. Generally, the higher the accuracy and rms wave perturbation, the larger the threshold value should be. To simplify the analysis and to make the analysis results of this study more comparable with previous studies, we take a fixed value of $10f$ for the threshold intrinsic frequency as was done in Vincent and Alexander (2000). Note that since both wind accuracies and rms wave perturbations may vary with stations and time, future studies need to be done to investigate the effects of varying the threshold intrinsic frequency on the analysis results.

It should be borne in mind that in this study the estimates of wave parameters and

vertical propagation direction were derived using polarization and dispersion relations for monochromatic gravity waves. Hence, the validity of this method is questionable to some extent when there exists a spectrum of waves. Also, note that generally gravity waves cover a very broad spectrum. In our radiosonde analysis, however, only those gravity waves with vertical wavelengths between 0.06-6.9 km for temperature and 0.3-6.9 km for wind can be detected if the derived mean profiles are assumed to be exact representations of the real background fields. In practice, the retrieval of the longest vertical wavelength (6.9 km) is not very well determined due to the use of second-order polynomial fits to remove the background fields[3]. This limitation of radiosonde observations must be borne in mind when comparing the analysis results from different types of data.

In the next section, the results on intrinsic frequency, vertical and horizontal wavelengths, and upward propagation direction derived from five years of U.S. high vertical resolution radiosonde data are presented.

[3]Alexander (1998) referred to such a limitation on the observable vertical wavenumber spectrum as the radiosonde's "observational filter".

3. Results

Wang and Geller (2003) analyzed four years (1998-2001) of U.S. high vertical resolution radiosonde data and found that gravity wave energies displayed certain spatial and temporal variations in both the troposphere and lower stratosphere. As will be shown in this section, important wave parameters such as intrinsic frequencies, vertical wavelengths, horizontal wavelengths, and fraction of upward energy propagation also exhibit distinctive spatial and temporal variations.

Intrinsic Frequency $\hat{\omega}$ Scaled by f

As described in section 2, the intrinsic frequency was derived from the axial-ratio of the wind perturbation hodograph. The upper panel of Fig. 1a shows the latitudinal distribution of five-year averaged (1998-2002) intrinsic frequencies $\hat{\omega}$ divided by the Coriolis parameter f in the troposphere (the red line and dots) and lower stratosphere (the black line and dots). The dots in the figure represent the values of $\hat{\omega}/f$ for each of the stations. For each individual dot (or station), the monthly means were calculated first. To ensure the representativeness of the monthly means, only those months which have at least 16 valid profiles are included in the calculation of means. The five-year averaged mean value was then calculated from the monthly means from January 1998 to December 2002. The lines are the latitudinal binned results of the dots with a bin size of 5°. The lower panel of Fig. 1a shows the monthly and zonally averaged[4] $\hat{\omega}/f$ for the lower stratospheric segment. As in the upper panel of Fig. 1a, the monthly

[4]As can be seen in Table 1 and Fig. 1 of Wang and Geller (2003), some latitudes have fewer stations than others. Also, the terrain may differ at some latitudes, so this presentation should be considered for what it is, an average of available station data in certain latitude bands.

means were calculated first for all of the stations. A 5° latitudinal bin is then used to bin the monthly means from the stations into a latitudinal grid from 5°N to 70°N. The blank region in the lower panel of Fig. 1a corresponds to 15°N and January 1998 and is caused by lack of valid soundings at that latitude and during that month. Finally, recall that those soundings that have intrinsic frequencies higher than $10f$ are removed before calculating the average, as noted in the previous section.

On the average, the lower stratospheric $\hat{\omega}/f$ decreases rather weakly from around 2.8 at 10°N to about 2.4 at 65°N. Meanwhile, there exists a local maximum of the ratio at mid-latitudes. As will be shown in Fig. 1c, such a local maximum results from higher values of $\hat{\omega}/f$ at several localized stations in the eastern U.S. It is evident from the lower panel of Fig. 1a that the latitudinal distribution of the ratio in summer is quite different from that in winter, with the latitudinal fall-off of the ratio with increasing latitude being more pronounced in summer and the localized maxima at mid-latitudes being more dominant in winter. The lower panel of Fig. 1a also shows that lower stratospheric ratio is exceptionally large at high-latitudes during the winter of 1999-2000.

The tropospheric ratio, on the other hand, displays much weaker latitudinal variations and has a value around 4. Also, no consistent latitudinal variations of the tropospheric ratio was found for the different months analyzed (not shown).

It is notable that $\hat{\omega}/f$ is higher in the troposphere than in the lower stratosphere by 30-60%, i.e., the tropospheric intrinsic frequency is higher than that in the lower stratosphere.

Since f is a stronger function of latitude (increasing with increasing latitude) than $\hat{\omega}/f$, Fig. 1a implies that the intrinsic frequency $\hat{\omega}$ actually increases with increasing

latitude in both the troposphere and lower stratosphere. In fact, $\hat{\omega}$ increases from roughly $7\times10^{-5}\ s^{-1}$ at 10°N to around $3.2\times10^{-4}\ s^{-1}$ at 65°N in the lower stratosphere and from $\sim 1\times10^{-4}\ s^{-1}$ at 10°N to around $5.3\times10^{-4}\ s^{-1}$ at 65°N in the troposphere. This means that the intrinsic period decreases from 24.9 hours at 10°N to 5.5 hours at 65°N in the lower stratosphere, and decreases from 17.5 hours at 10°N to 3.3 hours at 65°N in the troposphere.

As mentioned previously, Fig. 1a only shows the mean value of $\hat{\omega}/f$ when $1 < \hat{\omega}/f \leq 10$. It should be noted that the probability distribution of $\hat{\omega}/f$ has a distinctive peak at very low values of $\hat{\omega}/f$ ($1.3-1.7$ in the lower stratosphere and $1.6-2.5$ in the troposphere) with a tail extending to $\hat{\omega}/f = 10$ for all stations in both the troposphere and lower stratosphere (not shown). In addition, the peak is higher and tail smaller in the lower stratosphere than in the troposphere for all the stations.

It is evident from the lower panel of Fig. 1a that the lower stratospheric $\hat{\omega}/f$ (and $\hat{\omega}$) is larger in winter and smaller in summer at mid- and high-latitudes and displays considerable interannual variations at low-latitudes. The temporal variations of $\hat{\omega}/f$ can be seen more clearly in Fig. 1b where the monthly time series of the monthly and zonally averaged $\hat{\omega}/f$ in the troposphere and lower stratosphere at different latitudes ($10°-70°$N) are plotted. The thin solid lines are for the troposphere, whereas the thick solid lines are for the lower stratosphere. The thick dotted lines are the corresponding time series of background wind speeds (from the U.S. radiosondes) averaged over $18-24.9\ km$.

The tropospheric $\hat{\omega}/f$ varies very weakly with time and its temporal variations are difficult to characterize. In the lower stratosphere, the temporal variations of $\hat{\omega}/f$ at mid- and high-latitudes (north of 30°N) are dominated by an annual cycle

with maxima in DJF and minima in JJA. On the average, $\hat{\omega}/f$ is higher during DJF than during JJA by 40-50%. In the tropics (south of 10°N), the time series of the lower stratospheric $\hat{\omega}/f$ is dominated by interannual variations with DJF 1998-99 and 2000-01 having the highest frequencies, and the highest frequencies are larger than the lower ones by nearly 80%. Note that Wang and Geller (2003) find that the lower stratospheric total energy density E_t also exhibits considerable interannual variation at low-latitudes, which is related with QBO, i.e., E_t is strongest during the descent of the QBO westerly phase (DJF 1998-99 and 2001-02) and it is suppressed during the descent of the QBO easterly phase (1999-2000 and 2000-01 winters). The interannual variation of $\hat{\omega}/f$, however, does not match the interannual variation of the lower stratospheric E_t. The period of the former is shorter than that of the latter by about one year. At 20°N, there are no consistent temporal variations of the lower stratospheric ratio.

It is interesting that the linear correlation between the lower stratospheric $\hat{\omega}/f$ and wind speeds are positive and significant (at 95% confidence level) at all the latitudinal bands except for 20°N and 30°N. Such an apparent association between wind speeds and $\hat{\omega}/f$ will be discussed in section 4.

Fig. 1c shows the contoured maps of the seasonal means (DJF, MAM, JJA, and SON) of the tropospheric (the four lower panels) and lower stratospheric (the four upper panels) $\hat{\omega}/f$ averaged over five years (1998-2002). The blank regions in the troposphere are caused by the large number of discarded profiles for the tropospheric segment over Flagstaff, AZ as noted in the previous section.

The geographic distribution of the lower stratospheric ratio in the contiguous U.S. is characterized by higher values of the ratio over the east U.S., especially over Nor-

man, OK (35.2°N, 262.6°E), and Wilmington, OH (39.4°N, 276.3°E) for all seasons. On the other hand, the ratio is small over Nashville, TN (36.2°N, 273.4°E) and its surrounding stations for all seasons. The ratio is generally small over most of the western U.S. The geographic distribution of the tropospheric $\hat{\omega}/f$ is more complicated and is difficult to characterize, although generally the values are somewhat higher over part of the Rocky Mountains. Note that the geographic distributions of $\hat{\omega}/f$ in different seasons are consistent from year to year (not shown) and resemble those shown in Fig. 1c.

Vertical Wavelength

The most dominant vertical wavelength $\overline{\lambda}_z$ was estimated as the energy-weighted vertical wavenumber from the normalized temperature perturbation spectrum. Fig. 2a are similar to the upper panel of Fig. 1a, but for the most dominant vertical wavelength.

Distinctive latitudinal patterns can be seen for both the tropospheric and lower stratospheric $\overline{\lambda}_z$. In the troposphere, $\overline{\lambda}_z$ maximizes at about 45°N with a value of around 2.8 km, and it becomes slightly shorter south of 45°N. North of 45°N, the vertical wavelength also becomes shorter, and it takes a value of 2.3 km at 65°N. Note that there is a sharp decrease of $\overline{\lambda}_z$ from 50°N to 55°N. The sharp decrease is an artifact caused by the shorter altitude range specified for the Alaskan stations (i.e., 2-7.4 km as opposed to the normal 2-8.9 km). Because of the shorter altitude range in the Arctic, the lowest vertical wavenumber of the waves that can be resolved in the analysis becomes higher than in other regions. Hence, the mean vertical wavelength, which is inversely proportional to the mean vertical wavenumber, will be shorter. In

the lower stratosphere, $\overline{\lambda}_z$ decreases rather smoothly from 2.7 km at 10°N to around 2.2 km at 65°N.

Fig. 2b is similar to Fig. 1b, but for the time-series of the most dominant vertical wavelength. The thin- and thick-dotted lines in Fig. 2b are the corresponding time series of potential energy density Pe in the troposphere and lower stratosphere, respectively. It is evident from Fig. 2b that both the tropospheric and lower stratospheric $\overline{\lambda}_z$ are generally longer in winter than in summer. In addition, the seasonal variations of $\overline{\lambda}_z$ are generally bigger in the lower stratosphere than in the troposphere. On the average, $\overline{\lambda}_z$ is longer in winter than summer by 20-30% in the lower stratosphere, but its annual variation does not exceed 10% in the troposphere.

Fig. 2b also clearly shows a good correspondence between the time series of $\overline{\lambda}_z$ and that of Pe (except at 20°N and 30°N)[5] in the lower stratosphere.

Fig. 2c is similar to Fig. 1c, but for the geographic distribution of the most dominant vertical wavelength. In the troposphere, the principal maxima of the vertical wavelength are located over the Rocky Mountains for all seasons. In the lower stratosphere, the geographic distribution of $\overline{\lambda}_z$ is characterized by longer vertical wavelengths over most of the southeast U.S. except over Norman, OK and Wilmington, OH over which $\overline{\lambda}_z$ are instead localized minima for all seasons. The vertical wavelength is found to be generally short over the Rocky Mountains and northwest U.S. The geographic distribution of $\overline{\lambda}_z$ shown in Fig. 2c is consistent from year to year.

[5]This behavior at those latitudes needs to be investigated further.

Horizontal Wavelength

The most dominant horizontal wavelength $\overline{\lambda}_h$ was determined from $\hat{\omega}$ and $\overline{\lambda}_z$ for each sounding using the gravity wave dispersion relation. Fig. 3a is similar to Fig. 2a, but for $\overline{\lambda}_h$. It is obvious that $\overline{\lambda}_h$ decreases with increasing latitude in both the troposphere and lower stratosphere. For example, the tropospheric $\overline{\lambda}_h$ is about 600 km at 10°N, and it is around 75 km at 65°N. In the lower stratosphere, $\overline{\lambda}_h$ decreases from 2100 km at 10°N to about 300 km at 65°N. Note that the latitudinal gradient of $\overline{\lambda}_h$ is not uniform across the entire latitude range. In both the troposphere and lower stratosphere, $\overline{\lambda}_h$ drops off with latitude very steeply at low-latitudes. The latitudinal gradient becomes much smaller at higher latitudes. It is also worth noting that the lower stratospheric horizontal wavelength is ~ 3 times that in the troposphere throughout the whole latitude range.

Fig. 3b is similar to Fig. 2b but for the most dominant horizontal wavelength (the thick- and thin-solid lines). Also shown in the figure are the time series of the lower stratospheric Brunt-V*äisälä* frequency N at different latitudes (the thick-dotted lines). $\overline{\lambda}_h$ does not exhibit any consistent temporal variations in the troposphere. A clear annual cycle, however, can be seen in the lower stratosphere at mid-latitudes ($30° - 50°$N), where horizontal wavelengths in JJA are generally longer than those in DJF by 40-60%. At higher latitudes ($60° - 70°$N), the temporal variations are dominated by a semiannual cycle with the solstitial horizontal wavelengths being shorter than the equinoctial ones.

The geographic distribution of $\overline{\lambda}_h$ over the contiguous U.S. is obviously dominated by the the decreasing of horizontal wavelengths with increasing latitude. Secondary features such as relatively longer horizontal wavelengths over the eastern U.S. in

the troposphere, and relatively shorter vertical wavelengths over Norman, OK and Wilmington, OH in the lower stratosphere can also be clearly seen in Fig. 3c. The geographic distribution of $\overline{\lambda}_h$ shown in Fig. 3c is consistent from year to year.

Vertical Propagation Direction

The fraction of upward propagation was derived from the wind perturbation hodograph using the rotary spectral analysis method. Fig. 4a is similar to Fig. 2a, but for the fraction of upward energy propagation. In the troposphere, the fraction is slightly higher over Alaska and lower at low latitudes. In the lower stratosphere, the latitudinal distribution of the fraction shows a weak minimum at mid-latitudes. On the average, around 50% of the gravity wave energy propagates upward in the troposphere, whereas about 75% of the gravity wave energy propagates upward in the lower stratosphere.

Fig. 4b is similar to Fig. 1b, but for the fraction of upward energy propagation. The thick dotted lines in the figure are the corresponding time series of background wind speeds (from the U.S. radiosondes) averaged over the lower stratospheric segment (18-24.9 km), as in Fig. 1b. There is no consistent temporal variations of the tropospheric fraction. The lower stratospheric fraction, on the other hand, is generally smaller in DJF and bigger in JJA at mid- and high-latitudes (north of 30°N), and the seasonal variations can be as large as 30%. At low-latitudes, the temporal variations of the lower stratospheric fraction are roughly dominated by interannual variations with the winters of 1998-99, 2000-01, and 2001-02 having smaller fractions than other seasons. It is also worth noting that the lower stratospheric fraction at high latitudes (north of 50°N) is very much smaller during DJF 1999-2000 than during

other periods of time.

Fig. 4c is similar to Fig. 1c, but for the fraction of upward energy propagation. The principal feature in the geographic distribution of the fraction of upward gravity wave energy propagation is characterized by higher values over the lee side of the Rocky Mountains in the troposphere and over the windward side of the Rocky Mountains in the lower stratosphere. In addition, the lower stratospheric fraction is generally lower over Norman, OK, and Wilmington, OH, and higher over Nashville, TN. The geographic distribution of the fraction shown in Fig. 2c is consistent from year to year.

It is interesting that in the lower stratosphere, the local minima of this fraction over Norman, OK and Wilmington, OH and the local maximum over Nashville, TN (Fig. 4c), bear resemblance to the geographic distribution of $\overline{\lambda}_z$ (Fig. 2c) and $\overline{\lambda}_h$ (Fig. 3c), and are opposite to the geographic distribution of $\hat{\omega}/f$ (Fig. 1c) in the same region.

Finally, it should be recalled that the derived fractions of upward energy propagation are in fact underestimates of the real fractions due to the limitation of the rotary analysis method that was mentioned in section 2.

4. Discussion

As was shown in the previous section, the intrinsic frequencies scaled by f, the most dominant vertical and horizontal wavelengths, and the fractions of upward energy propagation, all exhibit distinctive spatial and temporal variations. It will be demonstrated in this section that most of the observed large scale and seasonal variations can be explained largely by the linear gravity wave dispersion relation, the latitudinal variation in the Coriolis parameter f, and/or background wind Doppler shifting. The lower stratospheric results are influenced a great deal by vertical energy propagation considerations. Source information is more easily seen in the troposphere. Perhaps then, specification of gravity wave sources in the troposphere may not be necessary for the parameterization of middle atmosphere gravity wave effects in global circulation models since propagation effects seem to dominate in the middle atmosphere.

Intrinsic Frequency $\hat{\omega}$ and $\hat{\omega}/f$

From the gravity wave dispersion relation (neglecting the density scale height term), the intrinsic frequency $\hat{\omega}$ is related to the Coriolis parameter f by

$$\hat{\omega}^2 = \frac{N^2\overline{K}^2 + f^2\overline{m}^2}{\overline{K}^2 + \overline{m}^2} = \frac{N^2\overline{K}^2/f^2 + \overline{m}^2}{\overline{K}^2 + \overline{m^2}} f^2 \tag{7}$$

Note that the maximum vertical wavelength that can be resolved in our analysis is 6.9 km, whereas the horizontal wavelength is at least hundreds of kilometers (see Fig. 3a) due to the fact that radiosondes are only detecting low intrinsic frequency waves (or long horizontal wavelength waves). This implies that $\overline{m} \gg \overline{K}$. Hence,

$$\hat{\omega}^2 - f^2 = N^2\overline{K}^2/\overline{m}^2 \tag{8}$$

Since N and $\overline{m}$ are not strong functions of latitude (Fig. 2a), we can infer from (8) that both $\hat{\omega}$ and $\overline{K}$ (or $1/\overline{\lambda}_h$) vary approximately linearly with f, as implied in Figs. 1a and 3a.

The derived intrinsic frequencies are generally very low, being around $4f$ in the troposphere and 2.4-3f in the lower stratosphere (Fig. 1a). Note that low intrinsic frequency gravity waves were also identified in previous analyses of radiosonde and rocket profiles (e.g., Hamilton 1991; Eckermann et al. 1994; Vincent et al 1997; Vincent and Alexander 2000). For example, in analyzing six years of radiosonde wind and temperature soundings over Cocos Islands, Vincent and Alexander (2000) found that the motion field appeared to be dominated by waves with frequencies of $2.7f$ in the lower stratosphere. The tendency for observing low frequency waves in radiosonde and rocket profiles may be in part due to the fact that these observational techniques can only detect relatively short vertical wavelength waves. Given the same horizontal wavelength, shorter vertical wavelengths lead to lower intrinsic frequencies, as can be inferred from (8).

The tendency for observing low intrinsic frequency waves may also be explained in part by the gravity wave vertical group velocity effect. The gravity wave vertical group velocity c_{gz} is given by

$$c_{gz} = -\frac{\hat{\omega}^2 - f^2}{\hat{\omega} m \left(1 + \frac{\hat{\omega}^2 - f^2}{N^2 - \hat{\omega}^2}\right)} \simeq -\frac{\hat{\omega}^2 - f^2}{\hat{\omega} m} \tag{9}$$

which implies that waves of higher intrinsic frequencies have larger vertical group velocities and thus gravity wave energy moves faster through a given altitude region. Fig. 5 shows the propagation time (in days) versus latitude for different intrinsic frequencies. In this plot, the propagation time is the time it would take a wave of a given frequency and a vertical wavelength of 2.5 km to travel vertically through

a 7-km-deep layer in the lower stratosphere. A typical lower stratospheric value of 0.02 s^{-1} was used for N to calculate the propagation time. It is evident from Fig. 5 that the propagation time depends strongly on the intrinsic frequency. The lower the intrinsic frequency, the longer it takes a wave to propagate through a given vertical distance. Note that the temporal sampling of radiosonde observations is only about twice daily, so they are more capable of capturing those waves which propagate very slowly, i.e., the low intrinsic frequency waves, if there is intermittency in the wave sources (as can be expected for convection generated waves for instance). So, since low intrinsic frequency waves are most likely to be observed, and since f defines the lowest frequency for gravity waves, it follows that the average $\hat{\omega}$ in these observations should show a strong dependence on f (Alexander et al. 2002).

In the lower stratosphere, the five-year averaged $\hat{\omega}/f$ decreases weakly from around 2.8 at 10°N to about 2.4 at 65°N. Similar (although larger) latitudinal variations of $\hat{\omega}/f$ have also been observed from CRISTA data (P. Preusse, private communication) and rocket observations (e.g., Hirota and Niki 1985). For example, Hirota and Niki (1985) found that in the altitude range of 30-60 km, $\hat{\omega}/f$ was in the range of $2.5 - 5$ and decreased with increasing latitude. Note that in their study, fluctuations with vertical scales between 1 and 15 km were obtained from rocket observations. The inclusion of larger vertical scale of motions in their study may explain the larger value of $\hat{\omega}/f$ than ours, as implied by (8).

The latitudinal variations of the lower stratospheric $\hat{\omega}/f$ may be explained conceptually by the vertical group velocity effect. Fig. 5 shows clearly that the vertical propagation time of a wave with a given intrinsic frequency decreases with increasing latitude. At lower latitudes, radiosondes cannot only detect the very low intrinsic

frequency (scaled by f) waves, they are also capable of capturing some higher intrinsic frequency (scaled by f) waves because at lower latitudes, these waves propagate slowly enough in the vertical for them to be well sampled by radiosondes. At higher latitudes, on the other hand, only the very low intrinsic frequency waves are slow enough for the temporal sampling of radiosondes. This may explain why the averaged $\hat{\omega}/f$ decreases with increasing latitude.

Of course, the latitudinal distribution of $\hat{\omega}/f$ can be complicated by the variations of wave intermittency and characteristics of different types of wave sources. This may lead to the the localized maximum of the lower stratospheric $\hat{\omega}/f$ at mid-latitudes in Fig. 1a which is due to the localized maxima over several stations in the eastern U.S., especially, Norman, OK and Wilmington, OH (Fig. 1c).

The larger values of $\hat{\omega}/f$ in the lower stratosphere at high-latitudes during DJF 1999-2000 (Fig. 1a) is probably due to the exceptionally strong background winds in that region during that time. For example, Fig. 6 shows the month-altitude contour of the monthly mean background wind speeds over Point Barrow, AK (71.3°N, 203.2°E) from the U.S. radiosondes. Note that the wind speeds have been smoothed in the vertical. It is obvious the wind is the strongest, exceeding 60 ms^{-1} in the lower stratosphere, during the winter of 1999-2000. Such a distribution of wind speeds as shown in Fig. 6 is typical for most of the other Alaskan stations (not shown). The especially strong lower stratospheric winds during DJF 1999-2000 act to Doppler shift low intrinsic frequency waves propagating upstream to higher intrinsic frequency waves, and hence are responsible for the higher values of $\hat{\omega}/f$ during DJF 1999-2000. This also implies that most waves propagate opposite to winds in that region and during that time, i.e., they propagate mostly westward. As will be shown in a

companion paper (Wang et al. 2004), waves indeed propagate roughly opposite to the background winds in the lower stratosphere.

The higher frequencies in the troposphere may be related to the fact that most gravity wave sources are located in that altitude region so that the considerations of vertical energy propagation are less important compared with the lower stratosphere. Another contributing effect is that there may be more trapping of higher intrinsic frequency waves in the troposphere. It is unclear at the moment what are the relative importance of the various causes of this troposphere-lower stratosphere difference.

Since stronger background wind speed generally tends to shift the intrinsic frequency of a wave propagating against the wind to a higher value, the high and positive correlations between the intrinsic frequency and background wind speed at mid- and high-latitudes suggest that the annual cycle of the lower stratospheric $\hat{\omega}/f$ is caused by the temporal variations of the background wind speed via the Doppler shift effect. Though smaller, the correlation is also significant at 95% confidence level at 10°N. The correlation is, however, insignificant at 20°N and 30°N. In addition to analyzing the latitudinal binned results, the correlation between the monthly time series of $\hat{\omega}/f$ and that of the background wind speed was also calculated for each individual station (not shown). Positive and significant correlations can be obtained for more than two-thirds of the total stations for the lower stratospheric segment. Best correlations are generally seen for stations located at mid- and high-latitudes (north of 40°N). Lower but still significant correlations are seen for most of the tropical stations. These provide strong evidence that the temporal variations of $\hat{\omega}/f$ are related with that of the background wind speeds. The correlation is generally poor for stations located between 15° and 35°N. In general, the correlation is insignificant for the tropospheric

segment.

The occurrences of higher intrinsic frequency waves in the lower stratosphere over several stations in the east U.S. such as Norman, OK and Wilmington, OH (Fig. 1c) cannot be explained by the background winds. Their cause(s) is (are) unknown at this time. The geographic distribution of $\hat{\omega}/f$ in the troposphere may indicate the source characteristics to a certain extent.

Vertical Wavelength

The vertical wavelengths that can be resolved in this study are severely limited by the vertical scale of radiosonde observations and the analysis method used, thus only relatively short vertical wavelength waves can be reliably retrieved from the U.S. radiosonde soundings.

It is interesting that the latitudinal distribution of the most dominant vertical wavelength $\overline{\lambda}_z$ (Fig. 2a) resembles that of the gravity wave total energy density E_t (Fig. 4 of Wang and Geller 2003). They both maximize at mid-latitudes in the troposphere and decrease with increasing latitude in the lower stratosphere. Note that the latitudinal distribution of both Pe and Ke (not shown) are also quite similar to that of E_t and $\overline{\lambda}_z$. The seemingly good correspondence between the latitudinal distribution of $\overline{\lambda}_z$ and gravity wave energy density can be explained schematically by Fig. 7 which shows two vertical wavenumber power spectra of gravity wave perturbations with energies of E_1 (solid curve) and E_2 (dashed curve), respectively, in energy-conservation coordinates. According to wave saturation theory, the tail (saturated) parts of the two spectra should have the same intensity if the Brunt-V*äisälä* frequency is assumed to be the same. It follows then that the energy-weighted vertical wavenumber (or

the mean vertical wavelength) for the solid curve should be smaller (larger) than that for the dashed curve. In other words, there should be a positive correlation between gravity wave energy and the energy-weighted vertical wavelength.

The annual cycle of the vertical wavelength in both the troposphere and lower stratosphere may also be related to the seasonal variations of gravity wave energies. Wang and Geller (2003) showed that gravity wave total energies are generally stronger in winter and weaker in summer in both the troposphere and lower stratosphere. It then follows that the vertical wavelength should also be longer in winter and shorter in summer in both regions. Fig. 2b shows that the time series of $\overline{\lambda}_z$ and Pe are indeed positively and significantly correlated except at 20°N and 30°N in the lower stratosphere. Note that the seasonal variations of gravity wave energies may also be related with the seasonal variations of the density and stability of the background atmosphere (Eckermann 1995).

The argument illustrated in Fig. 7 can also be applied to explain the longer vertical wavelengths over the Rocky Mountains in the troposphere. The local maxima over Norman, OK and Wilmington, OH and the local minima over Nashville, TN in the lower stratosphere, on the other hand, contradict the theoretical expectations. They may be artifacts due to the higher level of noise in the wind data in the lower stratosphere at some of these stations, but at the moment, the exact reason(s) for these discrepancies (are) not known.

It is interesting that the seasonal variations of the lower stratospheric $\overline{\lambda}_z$, $\hat{\omega}/f$, and winds are similar (Figs. 1b and 2b). The dispersion relation (8) can be used to show that seasonal changes in the wind could give positive correlations between $\overline{\lambda}_z$ and $\hat{\omega}/f$ for constant N and $\overline{\lambda}_h$. Correlations between $\overline{\lambda}_z$ and $\hat{\omega}/f$ are good at

Rocky Mountain stations, but generally poor elsewhere, suggesting other factors are also important.

Horizontal Wavelength

Manzini and McFarlane (1998) introduced a latitudinal dependence in the characteristic horizontal wavelength of the gravity wave source spectrum at the surface and at the 110 hPa pressure level (which is approximately 15 km in height, given a value of 7 km for the pressure scale height), on the assumption that the ratio of the model grid length to the effective gravity wave horizontal wavelength should vary relatively slowly in latitude. Their characteristic horizontal wavelength was specified to decrease from around 700 km at 10°N to around 300 km at 65°N. The latitudinal pattern of their horizontal wavelengths agrees with our results although the exact values are not the same.

The latitudinal distribution of $\overline{\lambda}_h$ was interpreted in the subsection on $\hat{\omega}$ in section 4 by the simplified dispersion relation (8), as for $\hat{\omega}$. Troposphere-stratosphere differences in $\overline{\lambda}_h$ are mainly due to larger values of N in the lower stratosphere than in the troposphere. On the average, the ratio of the lower stratospheric to the tropospheric N is ~ 2, while the ratio of the lower stratospheric to the tropospheric $\overline{\lambda}_h$ is ~ 3 (Figs. 4a and 4b). Hence, about one third of this differences is the result of other factors. Some of the differences might be accounted for by differences of the dominant vertical scales in the two regions.

According to the dispersion relation (8), $\overline{\lambda}_h$ should be proportional to N and $\overline{\lambda}_z$, and inversely proportional to $\hat{\omega}/f$. Figs. 1b, 2b, and 3b show that the seasonal variations of horizontal wavelengths are indeed positively correlated with those of N

and negatively correlated with those of $\hat{\omega}/f$ at mid-latitudes (e.g., 40°N), but they are negatively correlated with those of $\overline{\lambda}_z$, in contradiction to the theoretical expectation. This indicates that N and $\hat{\omega}$ dominate the seasonal variations of $\overline{\lambda}_h$ whereas the effect of $\overline{\lambda}_z$ on $\overline{\lambda}_h$ is negligible at mid-latitudes.

Finally, note that the consistency among horizontal wavelengths, vertical wavelengths, intrinsic frequencies and Brunt-V*äisälä* frequency should be expected since $\overline{\lambda}_h$ is derived from the other parameters using the gravity wave dispersion relation (6).

Vertical Propagation Direction

On the average, 50% wave energies propagate upward in the troposphere whereas 75% wave energies propagate upward in the lower stratosphere. This indicates that some waves might be generated in the upper troposphere and/or that tropospheric reflections of gravity waves are occurring.

Similar troposphere-lower stratosphere differences were also obtained by previous studies. For example, Vincent et al. (1997) found that typically $60-80\%$ of the wave energies propagate upward over Macquarie Island in the lower stratosphere. Eckermann et al. (1994) examined the rocket data in the $20-60$ km altitude range and found that the fraction was more than 50% in the lower stratosphere.

Zink and Vincent (2001) extracted gravity wave information from twice-daily radiosonde soundings over Macquarie Island between 1993 and 1995, and used the rotary spectral analysis to derive the vertical propagation direction. They found that the amount of wave energy propagating upward minimized in winter, agreeing with our results. On the other hand, Eckermann et al. (1994) found that the percentage of

upward propagation showed a marked semi-annual variation in the rocket data, with equinoctial maxima and minima at the solstices. In addition, they found that the winter minimum was almost always deeper than the summer one.

The temporal variations of the fraction of upward propagation in the lower stratosphere (winter minimum and summer maximum) from the U.S. radiosonde data can be interpreted by the variations of background winds. In general, the background winds are stronger in winter and weaker in summer, especially at mid- and high-latitudes. As mentioned before, stronger background winds tend to Doppler shift a gravity wave propagating against the wind to a higher intrinsic frequency. When the Doppler shifted intrinsic frequency reaches the reflection frequency (which is generally close to N), the wave's vertical group velocity will change sign and the wave will be reflected. Thus, there should be a negative correlation between the percentage of upward propagation and the strength of the background wind. In fact, such a negative relationship is clearly seen in Fig. 4b.

It is evident from Fig. 4b that the linear correlation between the time series of fraction of upward energy propagation and that of the background wind speed in the lower stratosphere is negative and significant for all the latitudinal bands except at 20° and 30°N, suggesting that the temporal variations of the fraction may be associated with the temporal variations of the background winds. Similar linear correlations were also calculated for all of the stations. Negative and significant correlations were found for more than 70% of the stations in the lower stratosphere (not shown). In addition, similar to what was found in the case of intrinsic frequencies vs. background winds, best (negative) correlations were generally seen for stations located at mid- and high-latitudes (north of 40°N). Negative and significant correlations were seen for

most of the tropical stations. The correlation is generally poor for stations located between 15°N and 35°N. The correspondence is poor in the troposphere.

In the lower stratosphere, the particularly small value of fraction at high latitudes (north of 50°) during DJF 1999-2000 (Fig. 4b) may also be associated with the exceptionally strong background winds in that region and during that time (e.g., Fig. 6). Note that Zink and Vincent (2001) also found the negative correspondence between background wind speed and the fraction of upward propagation over Macquarie Island.

In addition to propagation considerations, there are also gravity wave sources inside the troposphere and the sources will most likely vary with time. Thus, the temporal variations of the fraction of upward gravity wave energy propagation is more complicated in the troposphere, as shown in Fig. 4b. Note that the higher fractions over the Rocky Mountains in the troposphere (Fig. 4c) are consistent with topography being the major source of gravity waves over that region. Over other regions, gravity wave sources may probably be located at higher levels.

Figs. 4b and 1b indicate that the fraction of upward energy propagation is generally negatively and significantly correlated with $\hat{\omega}$ in the lower stratosphere. This is expected. As mentioned in section 2, the rotary analysis technique decomposes a single upward propagating wave into an upward-propagating part of $(1+f/\hat{\omega})/2$ fraction. Hence, the calculated fraction should be inversely proportional to $\hat{\omega}$ even when the true fraction remains a constant. It remains to be investigated to what extent the temporal variations of the calculated fraction of upward propagation reflect the temporal variations of the real fraction. Note that the correspondence between the time series of the tropospheric fraction and that of $\hat{\omega}$ is generally poor.

Data Quality

As noted in section 2, the U.S. radiosonde network wind soundings were measured by the Micro-ART (Micro computer Automated Radio Theodolite) system. Micro-ART utilizes a radio direction finding (RDF) antenna linked to a personal computer to record six second measurements of the azimuth and elevation angle of the radiosonde flight train. Details of the methods used to retrieve winds from the measurements of the azimuth and elevation angles can be found in the *Micro-ART Observation and Rework Programs Technical Document (NWS 1991)* and the *Data Documentation for Data Set Rawinsonde 6-second Data TD6211* (NCDC 2002).

Williams et al. (1993) and Miller and Blackmore (1995) noted the data quality of the six-second winds in the lower stratosphere deteriorates when the following instrument related problems occurs: (1) the elevation angles approach the elevation angle limit; and (2) the Micro-ART system fails to lock onto the radiosonde in a timely fashion so that spurious oscillations occur. The elevation angle problem is more serious in winter when the background wind is strong so that the elevation angle is generally low and is close to the elevation angle limit (normally 6°). Blackmore (private communication) also noted that two stations, i.e., Norman, OK and Wilmington, OH, are particularly susceptible to the above problems.

Fig. 8 shows examples of the original zonal (the thick solid line) and meridional (the thin solid line) wind sounding vs. altitude and the elevation angle sounding vs. the time since radiosonde release in the lower stratosphere ($18 - 24.9\ km$) over Norman, OK on January 1, 2001 0000 UTC. It is clear that the elevation angles of this flight are close to the elevation angle limit (6°). Hence, it is questionable whether the large perturbation in zonal wind is caused by data noise or is a real geophysical signal.

Note that this particular flight has passed the preliminary quality control procedure and has been included in the gravity wave analysis as was the case for many other soundings of this type at this location. Low elevation angles are also frequently seen in the soundings over Wilmington, OH, especially in winter (not shown).

Fig. 9 shows the time series of the normalized monthly mean background wind speed (the thick solid line), intrinsic frequency (the thin solid line), and fraction of upward propagation (the thin dashed line) in the lower stratosphere for Norman, OK and Wilmington, OH. In Fig. 9, the normalization of any time series Y is defined as follows:

$$Y' = \frac{Y - \frac{1}{2}(Y_{max} + Y_{min})}{\frac{1}{2}(Y_{max} - Y_{min})} \tag{10}$$

where Y_{max} and Y_{min} are the maximum and minimum values of Y, respectively. The above definition ensures that Y' is 1 if $Y = Y_{max}$, and -1 if $Y = Y_{min}$.

For Wilmington, OH, the time series of the wind speed is significantly and positively correlated with that of the intrinsic frequency, and is also significantly and negatively correlated with that of the fraction of upward propagation. These associations of wind speeds, intrinsic frequencies, and fraction of upward propagation are consistent with what we can expect from a monochromatic gravity wave, indicating that the information derived from the wind data over Wilmington, OH is likely related with real gravity wave signals. The correlations over Norman, OK, on the other hand, are insignificant [6]. The lack of correspondences over Norman, OK implies that the lower stratospheric wind data over Norman, OK may be distorted considerably by noise. It may also be caused by stronger wave-wave interaction or other nonlinear

[6] Calculations also show that the correlation between the lower stratospheric λ_z and Pe is significant over Wilmington, OH ($corr = 0.62$) and insignificant over Norman, OK ($corr = -0.05$)

processes over Norman, OK, for which a linear interpretation is not appropriate. Due to the lack of benchmark soundings to compare with, the exact extent to which the noise may affect the derived gravity wave information is difficult to assess at this time. Further investigation is needed to ascertain whether the abnormal behaviors of wave energies and parameters over Norman, OK are caused by data noise or are real geophysical signals.

To minimize the effect of data noise, for future work, we need to develop proper smoothing algorithms to filter out abnormally high level of noise in some of the lower stratospheric wind profiles and to extract as much geophysical information as possible and to minimize the noise contributions.

Note that the National Weather Service (NWS) is in the process of replacing the Micro-ART system with a GPS based radiosonde system, and hence the above problems related to tracking positions of radiosondes should be eliminated in the future.

5. Summary and Conclusions

Atmospheric gravity wave information has been derived from five years (1998-2002) of high vertical resolution U.S. radiosonde wind and temperature soundings for almost 90 stations. For each of the soundings, a tropospheric and lower stratospheric segment are selected for gravity wave analysis. Within each segment, gravity wave perturbations are estimated by subtracting a second-order polynomial fit from the original sounding. The derived wind and temperature perturbations are used to estimate gravity wave parameters such as the intrinsic frequency, the vertical and horizontal wavelengths, and the directions of vertical energy propagation. Distinctive spatial and temporal variations of these parameters have been found.

Consistent with previous studies, the most dominant gravity wave intrinsic frequency increases with increasing latitude in both the troposphere and lower stratosphere. This result is interpreted in terms of the gravity wave dispersion relation. Also, the lower stratospheric frequency is systematically less than the tropospheric one. This is a new result from our study. In the lower stratosphere, the intrinsic frequency is higher in winter and lower in summer, especially at mid- and high-latitudes. This is also a new result from our study, and is interpreted by the temporal variations of winds via the Doppler shift effect.

The most dominant intrinsic frequency divided by f has values around 4 in the troposphere, and $2.4-3$ in the lower stratosphere. Such low intrinsic frequency waves were also identified in previous analyses of radiosondes and rocket profiles. The tendency to observe low frequency waves in radiosonde profiles is likely caused by the fact that radiosondes can only detect relatively short vertical wavelength waves which have low intrinsic frequencies and by the limitation of temporal sampling of radiosondes.

In the lower stratosphere, $\hat{\omega}/f$ generally decreases weakly with increasing latitude. Such a latitudinal variation of $\hat{\omega}/f$ is consistent with the results of previous studies, and may be related to the gravity wave vertical group velocity effect and by the limitation of temporal sampling of radiosondes.

The most dominant vertical wavelength decreases with increasing latitude in the lower stratosphere, and maximizes at mid-latitudes (35°-40°N) in the troposphere. In both the troposphere and lower stratosphere, the vertical wavelengths are longer in winter and shorter in summer. These are new results from our study. The latitudinal and seasonal variations of vertical wavelengths are interpreted in terms of the dependence of the vertical wavelength on the gravity wave energy density.

The most dominant horizontal wavelength decreases with increasing latitude in both the troposphere and lower stratosphere, with larger values in the lower stratosphere. The latitudinal variation of horizontal wavelength is consistent with previous studies, and is shown to be a straightforward result of the gravity wave dispersion relation. The stratosphere-troposphere differences in horizontal wavelengths are caused mostly by the differences in the stability characteristics in the two different regions.

Approximately 50% of the tropospheric gravity waves show upward energy propagation, whereas there is about 75% upward propagation in the lower stratosphere, indicating that some waves might be generated in the upper troposphere and/or that tropospheric reflections of gravity waves are occurring. This is consistent with previous studies. The lower stratospheric percentage is generally smaller in winter and bigger in summer, especially at mid- and high-latitudes. This is also consistent with previous studies and may be interpreted in terms of stronger winds in winter which leads to more occurrences of wave reflection and weaker winds in summer resulting

in less wave reflection. The seasonal variations of the calculated fraction of upward propagation may also be an artifact caused by the limitation of the rotary analysis technique and the seasonal variations of $\hat{\omega}$. It is unknown at the moment how much of the temporal variations of the calculated fraction of upward propagation reflect the temporal variations of the real fraction.

As a critical note on the derived morphology of gravity wave parameters, it should be borne in mind that gravity waves have a wide spectrum, but radiosondes can only detect part of the spectrum, i.e., low intrinsic frequency and short vertical wavelength. The combination of the so called "observational filter" effect and the propagation of waves in the atmosphere renders the interpretation of the derived morphology of gravity wave activity in terms of wave sources less straightforward. Hence, it is not rigorously appropriate to apply directly the derived morphology of the parameters to the specification of gravity wave source spectra as used in GCMs' gravity wave parameterizations.

Also, we should be aware of the limit of the gravity wave analysis method used in this study. Many of the wave parameters are derived using the dispersion and polarization relations for a linear monochromatic wave. Hence, the analysis results are compromised in cases when we are dealing with a spectrum of waves. In addition, it is questionable whether the second-order polynomial fits truly represent the background fields, especially in the troposphere where it is difficult to separate the perturbations caused by gravity waves from those caused by temperature inversions and frontal systems.

Finally, the quality of the lower stratospheric wind data over some stations, in particular Norman, OK, seems to be to be sometimes poor. Further investigation

is needed to ascertain to what extent the abnormal behaviors of the derived wave energies and parameters over Norman, OK are caused by data noise or are real geophysical signals. Also, proper smoothing algorithms need to be developed to filter out abnormally high levels of noise in the lower stratospheric wind profiles due to limitations of the Micro-ART system in some cases.

In a companion paper, the results on the directions of horizontal propagation of gravity waves derived from the high vertical resolution U.S. radiosonde data will be presented.

Acknowledgment

The authors would like to thank Drs. Robert A. Vincent, Valery A. Yudin, and Steven D. Eckermann for helpful discussions with them regarding this paper. This research was funded by the U.S. National Science Foundation under grant ATM-1011039, Award 10447.

References

[1] Alexander, M. J., 1998: Interpretations of observed climatological patterns in stratospheric gravity wave variance, *J. Geophys. Res.,* **103,** 8627-8640.

[2] —, and R. A. Vincent, 2000: Gravity waves in the tropical lower stratosphere: A model study of seasonal and interannual variability, *J. Geophys. Res.,* **105,** 17 983-17 993.

[3] —, T. Tsuda, and R. A. Vincent, 2002: Latitudinal variations observed in gravity waves with short vertical wavelengths. *J. Atmos. Sci.,* **59,** 1394-1404.

[4] Allen, S., and R. A. Vincent, 1995: Gravity wave activity in the lower atmosphere: Seasonal and latitudinal variations, *J. Geophys. Res.,* **100,** 1327-1350.

[5] Andrews, D., J. Holton, and C. Leovy, 1987: *Middle Atmosphere Dynamics*, Academic Press, 489 pp.

[6] Durran, D. R., and J. B. Klemp, 1982: On the effects of moisture on the Brunt-Väisälä frequency, *J. Atmos. Sci.,* **39,** 2152-2158.

[7] Eckermann, S. D., and R. A. Vincent, 1989: Falling sphere observations of anisotropic gravity wave motions in the upper stratosphere over Australia. *Pure Appl. Geophys.,* **130,** 509-532.

[8] —, I. Hirota, and W. K. Hocking, 1994: Gravity wave and equatorial wave morphology of the stratosphere derived from long-term rocket soundings. *Q. J. R. Meteorol. Soc.,* **121,** 149-186.

[9] —, 1995: On the observed morphology of gravity-wave and equatorial-wave variance in the stratosphere. *J. Atmos. Terr. Phys.,* **57,** 105-134.

[10] —, and P. Preusse, 1999: Global measurements of stratospheric mountain waves from space. *Science,* **286**, 1534-1537.

[11] Fetzer, E. J., and J. C. Gille, 1994: Gravity wave variance in LIMS temperatures. Part I: Variability and comparison with background winds. *J. Atmos. Sci.,* **53,** 398-410.

[12] Fritts, D. C., and T. E. VanZandt, 1993: Spectral estimates of gravity wave energy and momentum fluxes. Part 1: Energy dissipation, acceleration, and constraints. *J. Atmos. Sci.,* **50,** 3685-3694.

[13] Fritts, D. C., and M. J. Alexander, 2003: Gravity wave dynamics and effects in the middle atmosphere. *Rev. Geophys.,* **41,** 10.1029/2001RG000106.

[14] Gossard, E. E., and W. H. Hooke, 1975: *Waves in the Atmosphere*, Elsevier Science, New York.

[15] Hamilton, K., 1991: Climatological statistics of stratospheric inertia-gravity waves deduced from historical rocketsonde wind and temperature data, *J. Geophys. Res.,* **96,** 20 831-20 829.

[16] —, and R. A. Vincent, 1995: High-resolution radiosonde data offer new prospects for research, *EOS,* **76,** 497.

[17] Haynes, P. H., C. J. Marks, M. E. McIntyre, T. G. Shepherd, and K. P. Shine, 1991: On the "downward control" of extratropical diabatic circulations by eddy-induced mean zonal forces, *J. Atmos. Sci.,* **48,** 651-678.

[18] Hines, C. O., 1989: Tropopausal mountain waves over Arecibo: A case study, *J. Atmos. Sci.,* **46,** 476-488.

[19] Hirota, I., 1984: Climatology of gravity waves in the middle atmosphere, *J. Atmos. Terr. Phys.,* **46,** 767-773.

[20] —, and T. Niki, 1985: A statistical study of inertia-gravity waves in the middle atmosphere. *J. Meteorol. Soc. Jpn,* **63,** 1055-1066.

[21] Holton, J. R., 1992: An Introduction to Dynamic Meteorology. *Academic Press,* 3rd ed. San Diego, 507 pp.

[22] —, P. H. Haynes, M. E. McIntyre, A. R. Douglass, R. B. Rood, and L. Pfister, 1995: Stratosphere-troposphere exchange, *Rev. Geophys.,* **33,** 403-439.

[23] Houghton, J. T., 1978: The Stratosphere and Mesosphere, *Q. J. Roy. Meteor. Soc.,* **104,** 1-29.

[24] Manzini, E., and N. McFarlane, 1998: The effect of varying the source spectrum of a gravity wave parameterization in a middle atmosphere general circulation model. *J. Geophys. Res.,* **103,** 31 523-31 539.

[25] McLandress, C., M. J. Alexander, and D. L. Wu, 2000: Microwave Limb Sounder observations of gravity waves in the stratosphere: A climatology and interpretation, *J. Geophys. Res.,* **105,** 11,947-11967.

[26] Medvedev, A., G. Klaassen, and S. Beagley, 1998: On the role of an anisotropic gravity wave spectrum in maintaining the circulation of the middle atmosphere. *Geophys. Res. Lett.,* **25,** 509-512.

[27] Miller, E., and W. Blackmore, 1995: A comparison of radiosonde windfinding techniques: Micro-ART and NEXUS (Loran-C Radionavigation). Preprints, *Ninth Symposium on Meteorological Observations and Instrumentation,* Charlotte, NC, Amer. Meteor. Soc., 49-54.

[28] Nastrom, G. D., T. E. VanZandt, and J. M. Warnock, 1997: Vertical wavenumber spectra of wind and temperature from high-resolution balloon soundings in the lower atmosphere over Illinois. *J. Geophys. Res.,* **102**, 6685- 6702.

[29] Nastrom, G. D., and T. E. VanzZandt, 2001: Seasonal variability of the observed vertical wave number spectra of wind and temperature and the effects of prewhitening. *J. Geophys. Res.,* **106,** 14,369-14,375.

[30] Scaife, A., N. Butchart, C. Warner, D. Stainforth, and W. Norton, 2000: Realistic quasi-biennial oscillations in a simulation of the global climate. *Geophys. Res. Lett.,* **27,** 3481-3484.

[31] Tsuda, T., M. Nishida, C. Rocken, and R. H. Ware, 2000: A global morphology of gravity wave activity in the stratosphere revealed by the GPS occultation data (GPS/MET), *J. Geophys. Res.,* **105,** 7257-7274.

[32] Vincent, R. A., 1984: Gravity-wave motions in the mesosphere. *J. Atmos. Terr. Phys.,* **46,** 119-128.

[33] —, S. J. Allen, and S. D. Eckermann, 1997: Gravity-wave parameters in the lower stratosphere. *Gravity Wave Processes: Their Parameterization in Global Climate Models,* K. Hamilton, Ed., Springer-Verlag, 7-25.

[34] —, and M. J. Alexander, 2000: An observational study of seasonal and interannual variability, *J. Geophys. Res.,* **105,** 17 971-17 982.

[35] Wang, L., and M. A. Geller, 2003: Morphology of Gravity Wave Energy as Observed from Four Years (1998-2001) of High Vertical Resolution U.S. Radiosonde Data, *J. Geophys. Res.,* **108,**, 10.1029/2002JD002786.

[36] Wang, L., M. A. Geller, and M. Joan Alexander, 2004: Spatial and temporal variations of gravity wave parameters. Part II: Horizontal propagation direction, to be submitted.

[37] Williams, S. F., C. G. Wade, and C. Morel, 1993: A comparison of high resolution radiosonde winds: 6-second Micro-ART winds versus 10-second CLASS LORAN winds. Preprints, *Eighth Symposium on Meteorological Observations and Instrumentation,* Anaheim, California, Amer. Meteor. Soc., 60-65.

[38] Zink, F., and R. A. Vincent, 2001: Wavelet analysis of stratospheric gravity wave packets over Macquarie Island 1. Wave parameters. *J. Geophys. Res.,* **106**, 10,275-10,288.

Table 1: The WBAN (Weather-Bureau-Army-Navy) ID numbers, station names, states, latitudes (deg N), and longitudes (deg E) of all the U.S. high vertical resolution radiosonde stations.

Station	Lat	Lon	Station	Lat	Lon
Pago Pago Intl Arpt, 99	-14.33	189.280	Sterling(Wash Dulles), VA	38.98	282.530
Ponape Island, 99	6.97	158.220	Topeka, KS	39.07	264.380
Majuro/Marshall Isl, 99	7.08	171.380	Grand Junction, CO	39.12	251.470
Koror/Palau IsLand, 99	7.33	134.480	Wilmington, OH	39.42	276.180
Truk Intl/Moen Isl, 99	7.47	151.850	Reno, NV	39.57	240.200
Yap Island, 99	9.48	138.080	Denver/Stapleton Arpt, CO	39.77	255.120
Seawell Apt, 99	13.07	300.500	Lincoln-Logan County Ap, IL	40.15	270.670
******, **[a]	13.5	144.800	Pittsburgh/Moon Township, PA	40.53	279.770
Guam, Mariana Is, 99	13.55	144.830	Salt Lake City, UT	40.77	248.030
Belize, 99	17.53	271.700	Elko, NV	40.87	244.270
San Juan/Isla Verde, PR	18.43	294.000	Brookhaven, NY	40.87	287.130
Grand Cayman, 99	19.30	278.630	North Platte, NE	41.13	259.320
Hilo, HI	19.72	204.930	Omaha/Valley, NE	41.32	263.630
Lihue/Kauai, HI	21.98	200.650	Davenport Municipal Ap, IA	41.60	269.430
******, **[b]	24.50	278.200	Chatham, MA	41.67	290.030
Miami/FL Intl Univ, FL	25.75	279.620	Medford, OR	42.37	237.130
Brownsville, TX	25.90	262.570	Detroit/Pontiac, MI	42.70	276.530
Tampa Bay/Ruskin, FL	27.70	277.600	Buffalo/Grtr Arpt, NY	42.93	281.270
Corpus Christi, TX	27.77	262.500	Riverton, WY	43.06	251.530
Del Rio, TX	29.37	259.080	Boise, ID	43.57	243.780
Lake Charles, LA	30.12	266.780	Gray, ME	43.89	289.750
Slidell, LA	30.33	270.180	Rapid City, SD	44.07	256.790
Tallahasee, FL	30.38	275.630	Green Bay, WI	44.48	271.870
Jacksonville, FL	30.43	278.300	Gaylord / Alpena, MI	44.55	275.570
Santa Teresa, NM	31.90	253.300	Minneapolis, MN	44.83	266.450
Midland, TX	31.93	257.800	Salem, OR	44.92	236.980
Tuscon, AZ	32.12	249.070	Aberdeen, SD	45.45	261.580
Jackson/Thompson Fld, MS	32.32	269.930	Bismarck, ND	46.77	259.250
Shreveport Regional Ap, LA	32.45	266.170	Caribou, ME	46.87	291.980
Ft Worth, TX	32.80	262.700	Great Falls, MT	47.45	248.620
Miramar Nas, CA	32.87	242.850	Spokane Intnl Apt, WA	47.68	242.370
Charleston, SC	32.90	279.970	Quillayute, WA	47.95	235.450
Birmingham (Shelby Apt), AL	33.10	273.300	Glasgow, MT	48.20	253.380
Peachtree City, GA	33.35	275.440	International Falls, MN	48.57	266.620
Morehead City/Newport, NC	34.70	283.200	Annette Island, AK	55.03	228.430
N Little Rock, AR	34.83	267.730	Cold Bay, AK	55.20	197.280
Albuquerque, NM	35.05	253.380	St Paul Island, AK	57.15	189.780
Norman, OK	35.23	262.530	Kodiak, AK	57.75	207.520
Amarillo, TX	35.23	258.300	King Salmon, AK	58.68	203.350
Flagstaff/Bellemt(Army), AZ	35.23	248.180	Yakutat, AK	59.52	220.330
Greensboro, NC	36.08	280.050	Bethel, AK	60.78	198.200
Nashville, TN	36.25	273.430	Anchorage Iap/Pt. Campbe, AK	61.17	209.980
Desert Rock/Mercury, NV	36.62	243.980	Mcgrath, AK	62.97	204.380
Roanoke/Blacksburg, VA	37.20	279.590	Nome Ap, AK	64.50	194.570
Springfield Regional Ap, MO	37.23	266.600	Fairbanks, AK	64.82	212.130
Oakland Int Ap, CA	37.75	237.780	Kotzebue, AK	66.87	197.370
Dodge City, KS	37.77	260.030	Point Barrow, AK	71.30	203.220

[a]The corresponding WBAN number is 12850.
[b]The corresponding WBAN number is 41406.

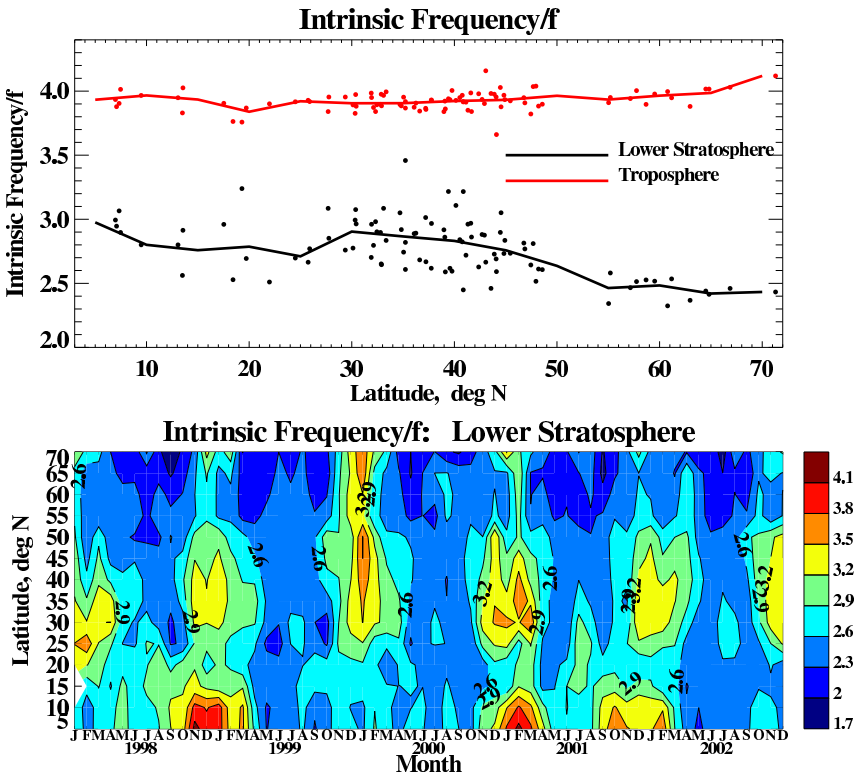

Fig. 1a: Upper panel: five-year (1998-2002) averaged intrinsic frequencies divided by the Coriolis parameter f for each of the radiosonde stations as a function of latitude in the troposphere (red dots) and lower stratosphere (black dots). The red and black solid lines are the latitudinal binned results (with a bin size of 5°) for the troposphere and lower stratosphere, respectively. Lower panel: the month-latitude contour of monthly and zonally averaged intrinsic frequencies divided by f in the lower stratosphere. The contour interval is 0.3. See text for details.

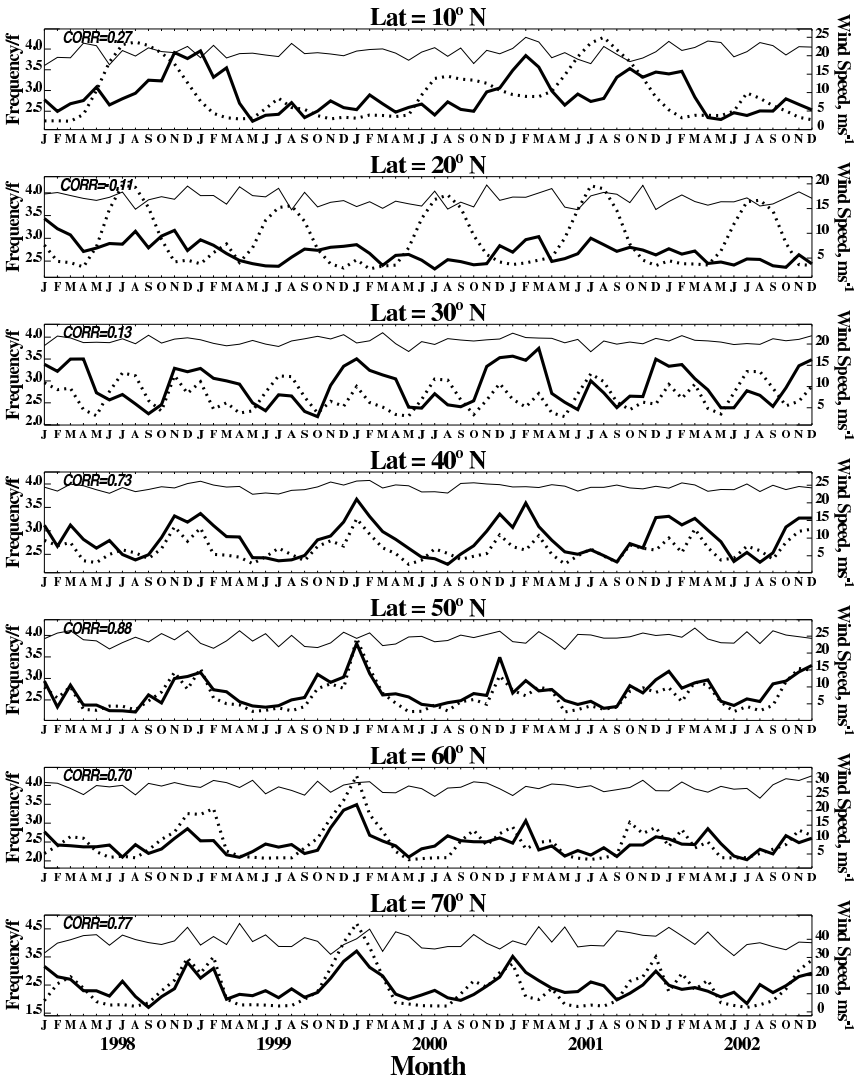

Fig. 1b: Monthly time series of the monthly and zonally averaged intrinsic frequency divided by f in the troposphere (the thin solid lines) and lower stratosphere (the thick solid lines) at different latitudes ($10^\circ - 70^\circ$N). Also shown are the monthly time series of background wind speeds (ms^{-1}) averaged over 18-24.9 km (the thick dotted lines). See text for details.

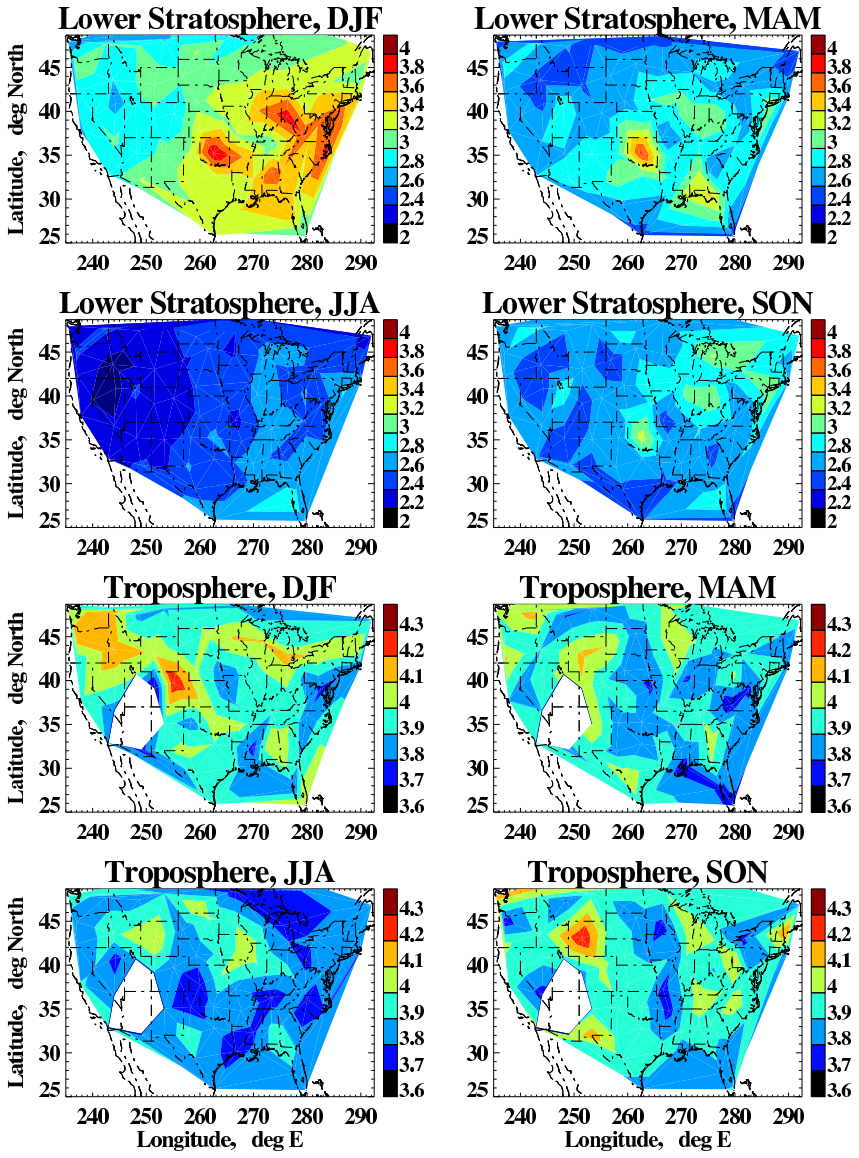

Fig. 1c: Contoured maps of five-year (1998-2002) averaged seasonal means (DJF, MAM, JJA, and SON) of tropospheric and lower stratospheric intrinsic frequencies divided by f over the contiguous United States. The contour interval is 0.1 for the troposphere (the four lower panels) and 0.2 for the lower stratosphere (the four upper panels).

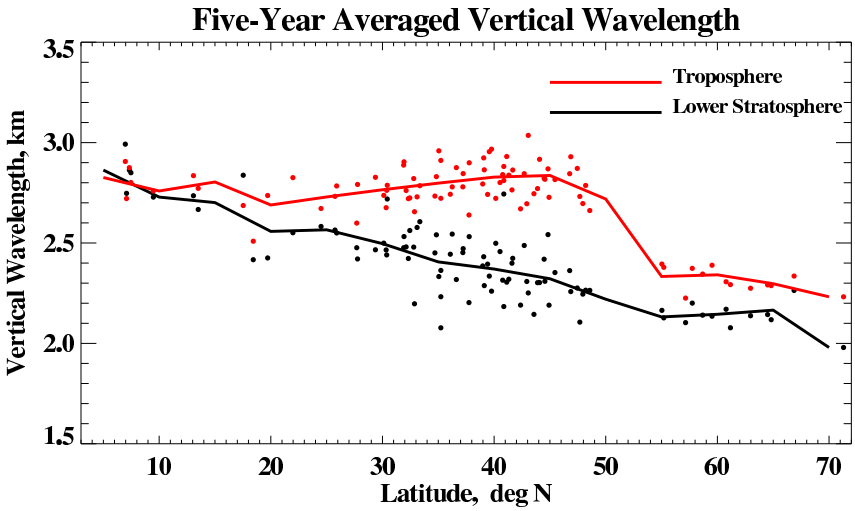

Fig. 2a: Same as the upper panel of Fig. 1a, but for the most dominant vertical wavelength (km).

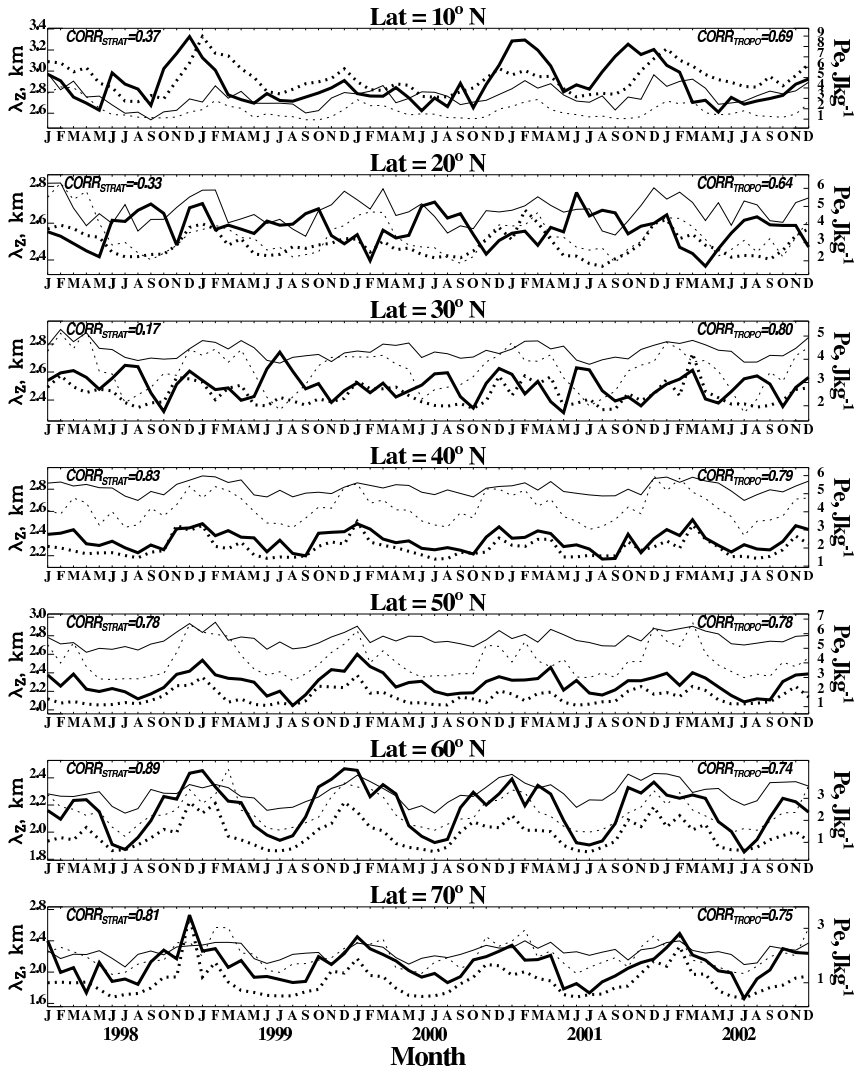

Fig. 2b: Similar to Fig. 1b, but for the most dominant vertical wavelength (km). The thin- and thick-dotted lines are the corresponding time series of potential energy density (Jkg^{-1}) in the troposphere and lower stratosphere, respectively.

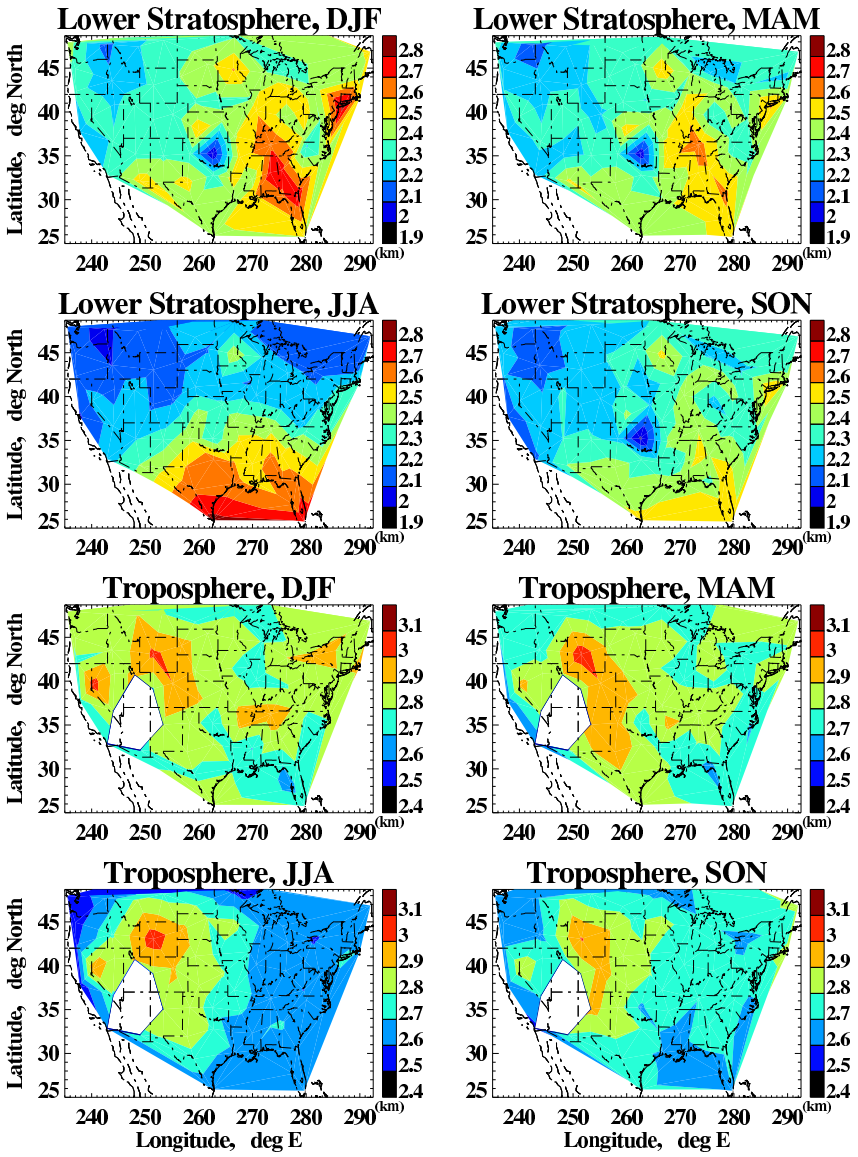

Fig. 2c: Same as Fig. 1c, but for the most dominant vertical wavelength. The contour interval is 0.1 km.

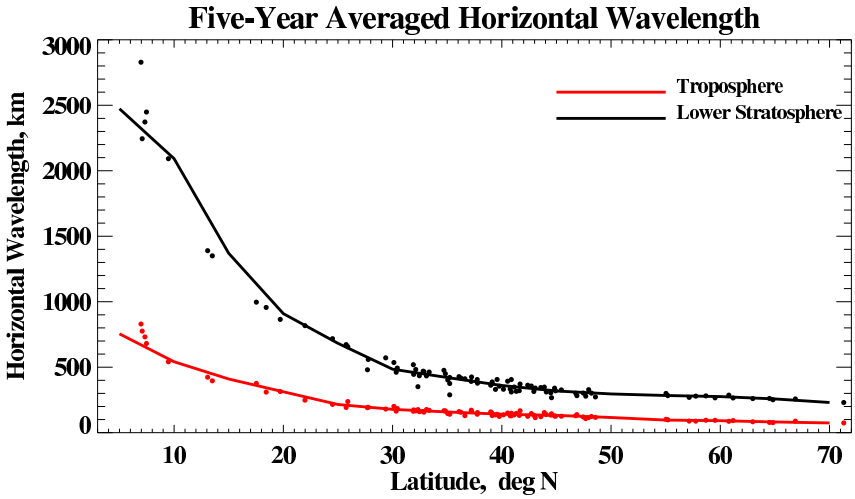

Fig. 3a: Same as Fig. 2a, but for the most dominant horizontal wavelength (km).

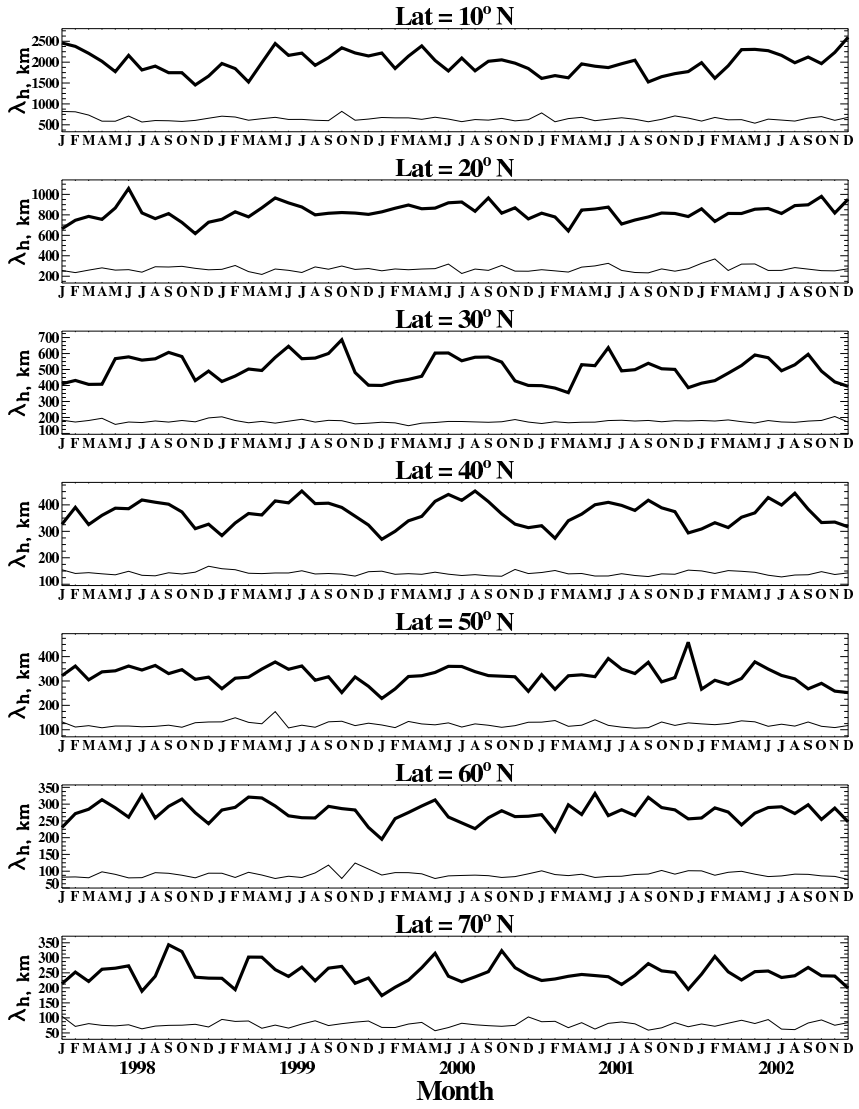

Fig. 3b: Similar to Fig. 1b, but for the most dominant horizontal wavelength (km).

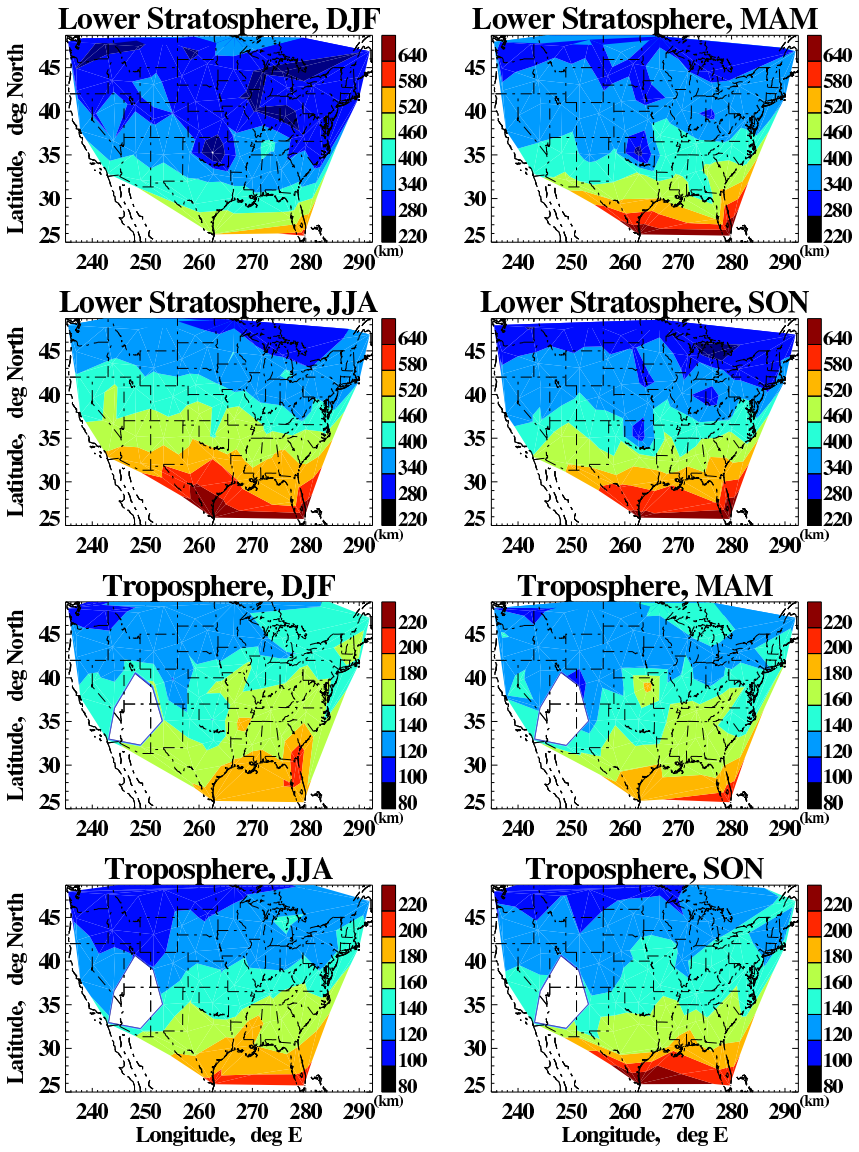

Fig. 3c: Same as Fig. 1c, but for the most dominant horizontal wavelength. The contour interval is 20 km for the troposphere (the four lower panels), and 60 km for the lower stratosphere (the four upper panels).

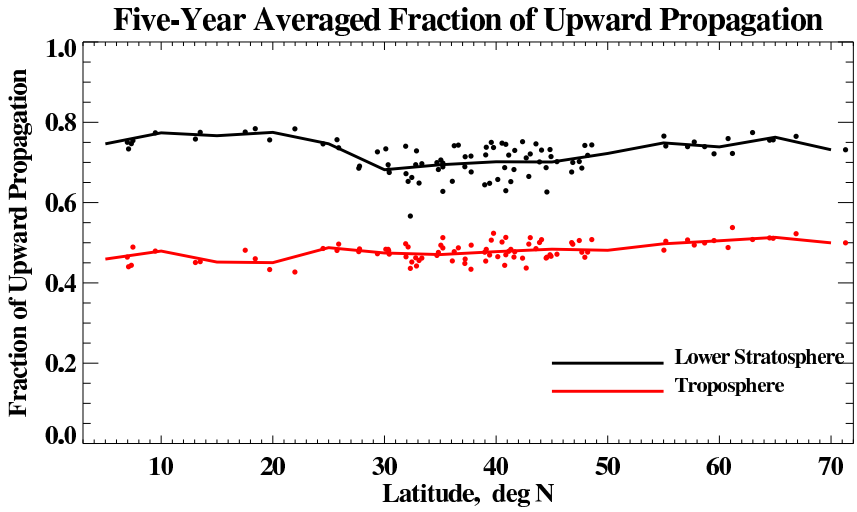

Fig. 4a: Same as Fig. 2a, but for the fraction of upward energy propagation.

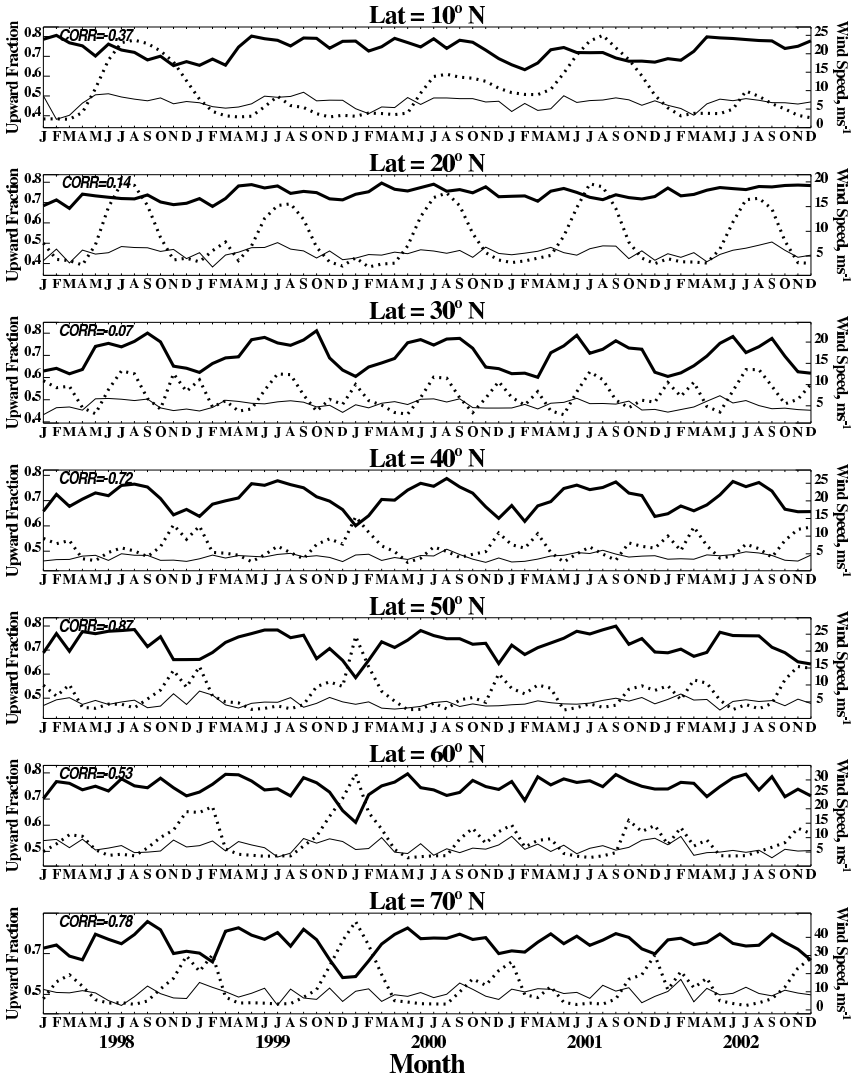

Fig. 4b: Similar to Fig. 1b, but for the fraction of upward energy propagation. The thick-dotted lines are the monthly time series of background wind speeds (ms^{-1}) averaged over 18-24.9 km.

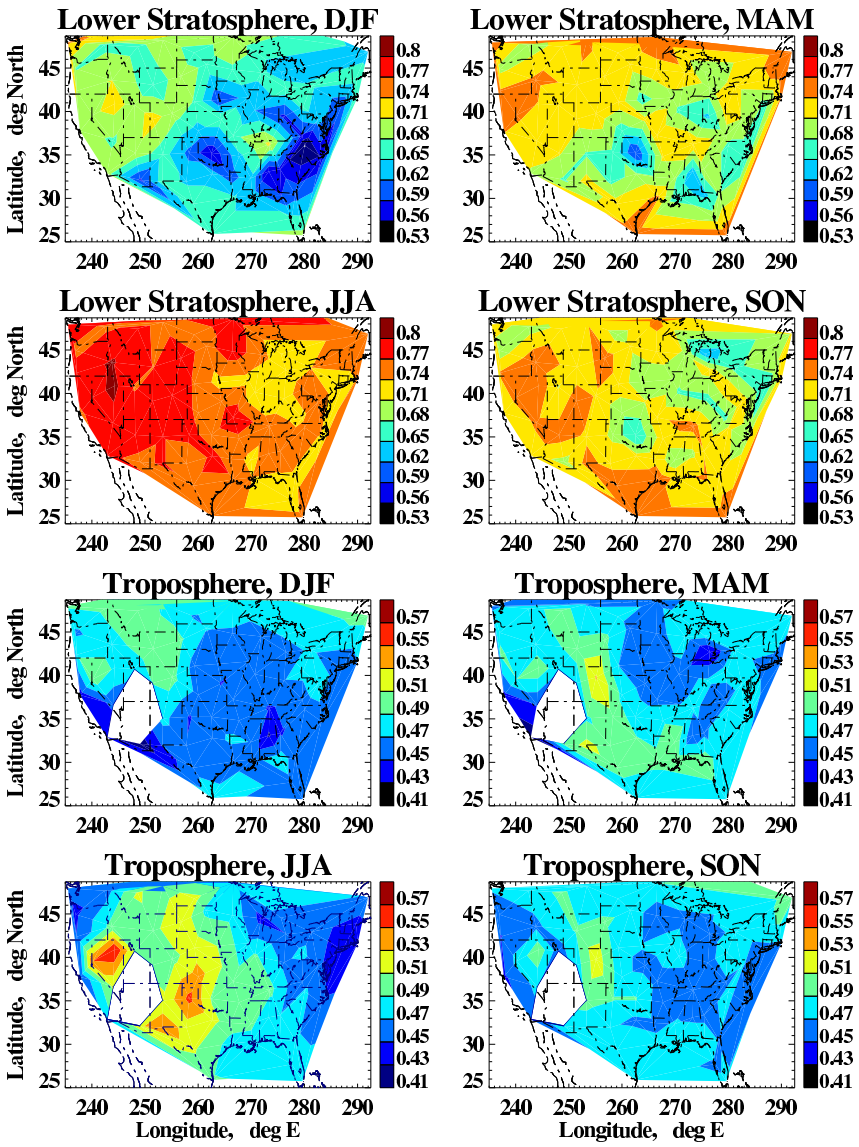

Fig. 4c: Same as Fig. 1c, but for the fraction of upward energy propagation. The contour interval is 0.02 for the troposphere (the four lower panels), and 0.03 for the lower stratosphere (the four upper panels).

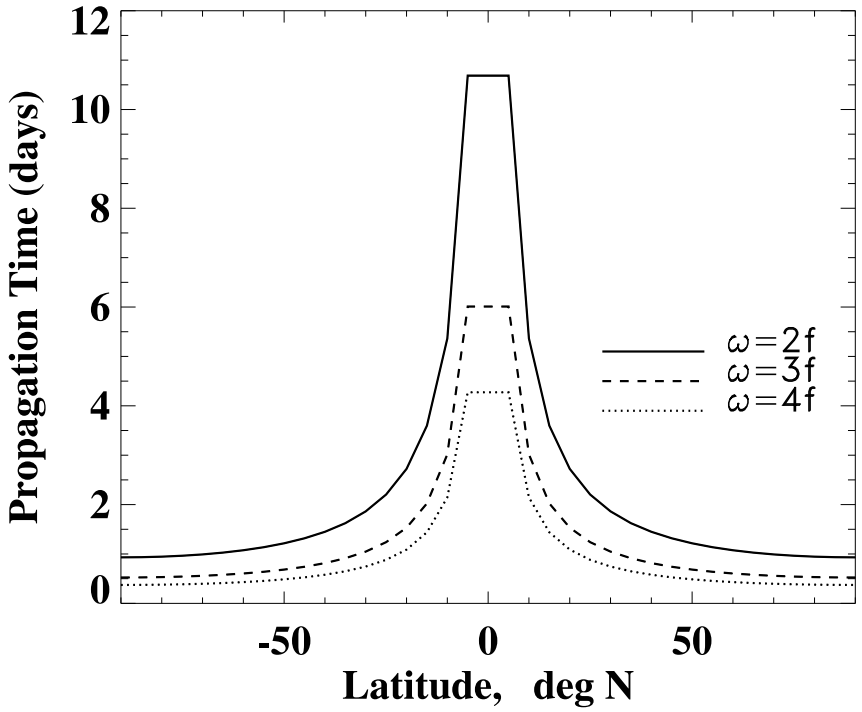

Fig. 5: Propagation time (in days) versus latitude for different intrinsic frequencies. The propagation time is the time it would take a wave of a given frequency and a vertical wavelength of 2.5 km to travel vertically through a 7-km-deep layer in the lower stratosphere.

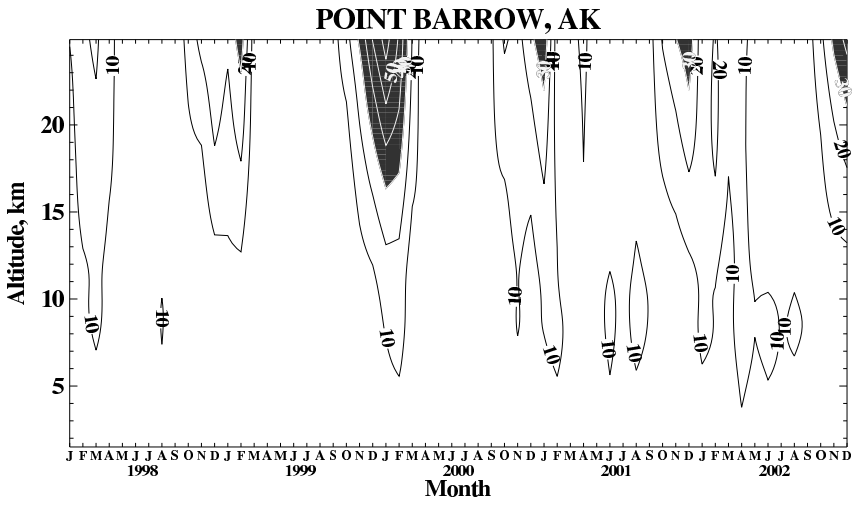

Fig. 6: The month-altitude contour of the monthly mean background wind speed over Point Barrow, AK (71.3°N, 203.2°E) (from U.S. radiosondes). The contour interval is 10 ms^{-1}. The part where the wind speed exceeds 30 ms^{-1} is shaded.

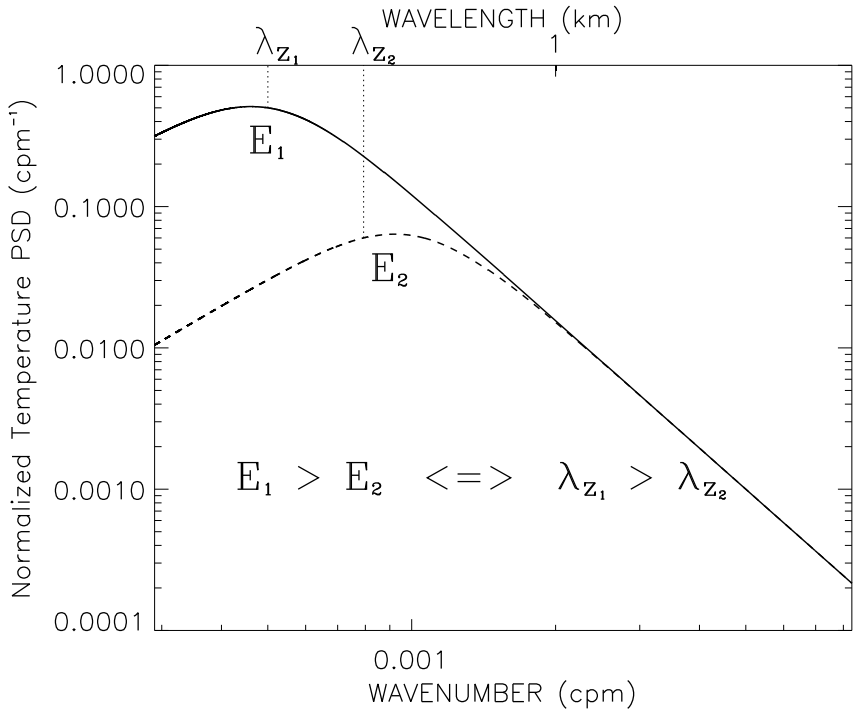

Fig. 7: Schematic showing vertical wavenumber power spectra of gravity wave perturbations with variances of E_1 and E_2, respectively, in energy-conserved form.

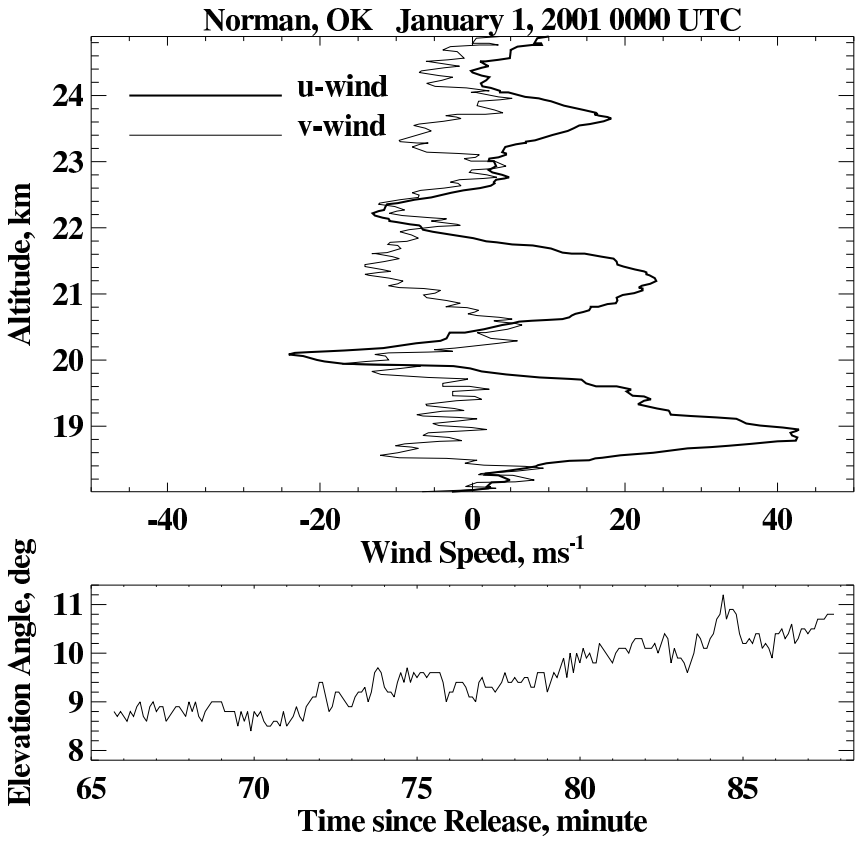

Fig. 8: Upper panel: the original zonal and meridional wind components (ms^{-1}) for the flight on January 1, 2001 0000 UTC over Norman, OK (35.2°N, 262.6°E) in the lower stratosphere. Lower panel: the corresponding time since balloon release (in minutes) vs. elevation angle (in degrees) plot. See text for details.

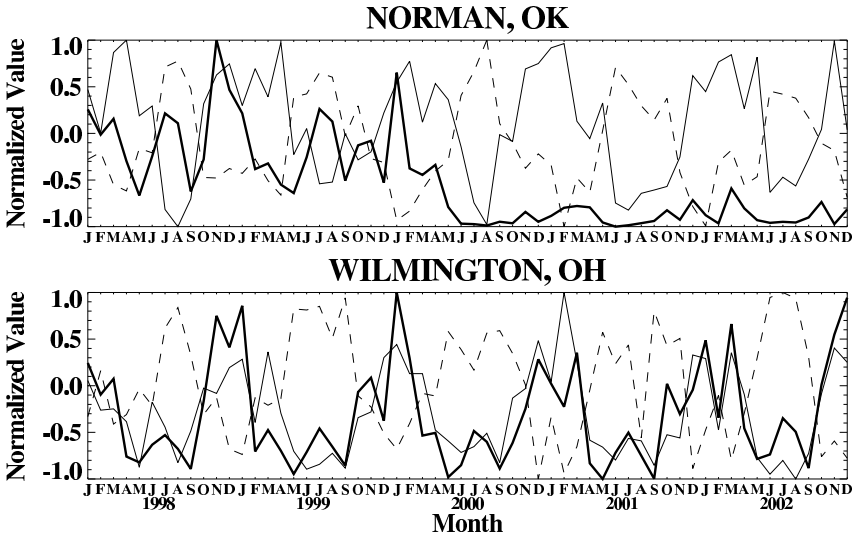

Fig. 9: Time series of the normalized monthly mean background wind speed (the thick solid lines), intrinsic frequency (the thin solid lines), and fraction of upward propagation (the thin dashed lines) in the lower stratosphere for Norman, OK (35.2°N, 262.6°E) (the upper panel) and Wilmington, OH (39.4°N, 276.3°E) (the lower panel). See text for details.